iScience

CellPress
OPEN ACCESS

Article

Spatial and temporal characteristics of laboratory-induced *Anopheles coluzzii* swarms: Shape, structure, and flight kinematics

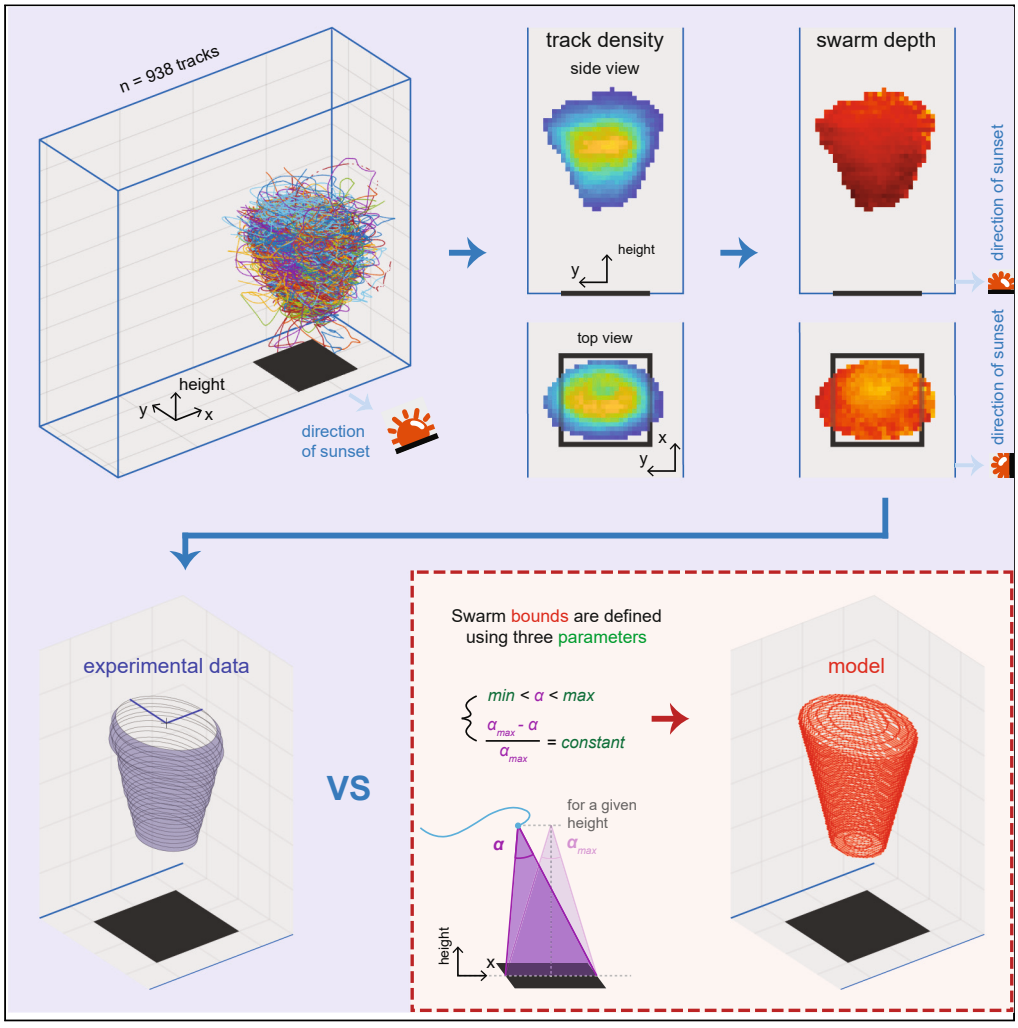

Bèwadéyir Serge Poda, Antoine Cribellier, Lionel Feugère, ..., Abdoulaye Diabaté, Florian T. Muijres, Olivier Roux

sergepoda71@yahoo.fr

Highlights

Three-dimensional kinematics of malaria mosquitoes swarms during simulated sunset

Swarms are stereotypically shaped as an elliptical cone above a visual swarm marker

Flight kinematics varies spatially throughout the swarm volume, but not with time

Mosquitoes use visual perception of the swarm marker and sunset horizon to swarm

Poda et al., iScience 27, 111164
November 15, 2024
https://doi.org/10.1016/j.isci.2024.111164

iScience

CellPress
OPEN ACCESS

Article

Spatial and temporal characteristics of laboratory-induced *Anopheles coluzzii* swarms: Shape, structure, and flight kinematics

Bèwadéyir Serge Poda,[1,2,3,4,10,11,*] Antoine Cribellier,[4,10] Lionel Feugère,[5,6] Mathurin Fatou,[7,8] Charles Nignan,[1,2,9] Domonbabele François de Sales Hien,[1] Pie Müller,[7,8] Olivier Gnankiné,[2] Roch Kounbobr Dabiré,[1] Abdoulaye Diabaté,[1] Florian T. Muijres,[4] and Olivier Roux[1,3]

SUMMARY

Malaria mosquitoes mate in swarms, but how these swarms are formed and maintained remains poorly understood. We characterized three-dimensional spatiotemporal flight kinematics of *Anopheles coluzzii* males swarming at sunset above a ground marker. The location, shape, and volume of swarms were highly stereotypic, consistent over the complete swarming duration. Swarms have an elliptical cone shape; mean flight kinematics varies spatially within the swarm, but remain rather consistent throughout swarming duration. Using a sensory system-informed model, we show that swarming mosquitoes use visual perception of both the ground marker and sunset horizon to display the swarming behavior. To control their height, swarming individuals maintain an optical angle of the marker ranging from 24° to 55°. Limiting the viewing angle deviation to 4.5% of the maximum value results in the observed elliptical cone swarm shape. We discuss the implications of these finding on malaria mosquito mating success, speciation and for vector control.

INTRODUCTION

Malaria mosquitoes are among the world's deadliest animals. Each year, they cause millions of *Plasmodium* infections in humans and hundreds of thousands of human deaths.[1] The primary malaria prevention method is to limit mosquito biting through vector control, which is mainly based on the use of insecticides through treated bed nets and indoor residual spraying.[2,3] These vector control methods are increasingly under pressure due to the ongoing rise in insecticide resistance in mosquitoes.[4,5] Consequently, further reduction of malaria cannot be achieved using insecticide-based prevention methods alone. Instead, in a context of integrated vector management, for effective malaria control, these conventional control methods need to be augmented with alternative complementary methods.[6–8]

Alternative complementary methods based on mating biology are currently being developed for effective control of malaria and dengue in a broader context of vector-borne disease control. Promising candidates are sterile insect technique,[9,10] genetically modified mosquitoes,[11,12] or incompatible insect technique.[13,14] The effectiveness of these control techniques is strongly linked to the ability of the modified mosquitoes to mate successfully with wild individuals. Consequently, the development of these methods requires a good knowledge of the mating biology and ecology of target mosquitoes.[15,16] Unfortunately, we have currently limited knowledge of mosquito mating behavior.

Anopheles mosquitoes are known to mate mainly in-flight in outdoor swarms. Mating swarms are formed by males at sunset, usually above a visual ground marker, and females fly into the swarm to find a mate.[17–19] However, the processes of how male mosquitoes form and maintain a swarm, as well as their flight behavior in the swarm remain largely unknown.[16,19–21] This limited knowledge is partly due to the difficulty to study the behavior of relatively small insects (~5 mm), under outdoor low light conditions (~3–5 lux), in a relatively short time period per day (~20 min), and in large aggregations of individuals (up to thousands of males) in which individuals fly fast (about 0.2–2 m/s).[17–19,22,23] As a result, previous studies based on direct observations have provided limited data on *Anopheles* swarming and mating behavior.

[1]Département de Biologie Médicale et Santé Publique, Institut de Recherche en Sciences de la Santé, Bobo-Dioulasso, Burkina Faso
[2]Laboratoire d'Entomologie Fondamentale et Appliquée, Unité de Formation et de Recherche en Sciences de la Vie et de la Terre, Université Joseph KI-ZERBO, Ouagadougou, Burkina Faso
[3]MIVEGEC, IRD, CNRS, University of Montpellier, Montpellier, France
[4]Experimental Zoology Group, Wageningen University and Research, Wageningen, the Netherlands
[5]Natural Resources Institute, University of Greenwich, Chatham, UK
[6]L2TI, Université Sorbonne Paris Nord, Villetaneuse, France
[7]Swiss Tropical and Public Health Institute, Allschwil, Switzerland
[8]University of Basel, Basel, Switzerland
[9]Unité de Formation et de Recherche en Sciences Appliquées et Technologies, Université de Dédougou, Dédougou, Burkina Faso
[10]These authors contributed equally
[11]Lead contact
*Correspondence: sergepoda71@yahoo.fr
https://doi.org/10.1016/j.isci.2024.111164

Experimental approaches using machine-vision-based tracking systems in controlled laboratory or semi-field conditions can at least partially resolve these limitations, as such an approach can provide quantitative data on the movement kinematics of swarming mosquitoes in controlled conditions. The first videography-based studies focused on two-dimensional trajectories or three-dimensional positions of swarming mosquitoes in natural or laboratory-induced swarms.[17,24–26] Recent advancements in machine-vision with high spatial and temporal resolution videography, and automatized tracking techniques have increased the degree of automation in data collection.[27–29] This allowed for multi-target tracking of the three-dimensional trajectories of swarming mosquitoes,[23,30–32] and have made available large datasets for in-depth analyses.[33,34]

These studies provided a quantitative description of several important traits of mating swarms that could be useful in assessing the 'quality' of mosquito strains in mosquito release-based methods of vector control,[32] or raise further avenues in explaining the speciation process and the diversification in the *Anopheles gambiae* complex.[23,26,30,31] However, important questions are still unanswered, particularly with respect to the temporal and spatial dynamics of swarming, and how the swarming mosquitoes interact with environmental cues such as the visual ground marker and sunset cues.

Here, we assessed these questions by studying experimentally induced swarms of male *Anopheles coluzzii* mosquitoes, a primary vector of malaria in West Africa. We used a custom-built videography-based tracking system that records the three-dimensional motion of swarming individuals. Based on these flight kinematics, we reconstructed the kinematics of the swarm as a whole, and determined how these swarm kinematics change throughout three swarming periods: at swarm formation, at the peak swarming activity, and at the end of swarming; and we quantified how this relates to the swarm marker and sunset cues. Finally, we developed a sensory-cue-inspired model that describes how swarm location, shape and size depend on visual input in the swarming male mosquitoes. The analysis of these data enabled us to formulate further hypotheses on swarming and mating behavior in *Anopheles* mosquitoes.

RESULTS

Mosquito flight activity differs across the swarming phases

The experimental set-up allowed for filming in three-dimensions across the complete flight arena, and therefore the recording of all flight behavior of mosquitoes during the swarming period (Figures S1A–S1C). Mosquito flight behavior exhibited a consistent pattern. As the ceiling lights dimmed, mosquitoes predominantly rested on the walls of the flight arena before initiating random flights approximately 2 min prior to lights-off (Figure 1C). Two to 3 min after the ceiling lights turned off, a male started to fly repeatedly over the marker. In five of the six experiments, additional mosquitoes joined the swarm within 7–90 s (t_{start} = 46 ± 8 s; mean ± se, n = 5 experiments out of six in total). In one of the six experiments, the first male swarmed alone for 233 s before departing the swarm location. The number of swarming mosquitoes steadily increased, reaching a swarming peak about 10 min later, during which the majority of flying individuals were engaged in swarming activity. This peak was relatively stable for approximately 20 min, after which the number of swarming mosquitoes gradually decreased back to zero (Figure 1C). It is worth noting that mosquitoes flying outside the swarm at the ending phase were flying mainly along the walls of the flight arena, bouncing against the walls as an apparent escape behavior.

During the recordings, 18%–73% of released mosquitoes showed flight activity, and 4%–54% of them exhibited swarming behavior. To systematically test how flight activity varied throughout the swarming period, we compared both the flight and swarming activity across the three swarming phases (start, peak and ending phase; Figure 1C and Table S1). This shows that both the number of flying mosquitoes and the number of swarming mosquitoes were statistically different between the three phases (Table S1). While the number of flying mosquitoes at the start and the end phases did not differ significantly, the number of flying mosquitoes was significantly higher during the peak phase compared to both the start and end phases (start: n_{flying} = 15.5 ± 2.1 mosquitoes; peak: n_{flying} = 23.3 ± 2.3; end: n_{flying} = 14.0 ± 2.4; Table S1). Likewise, the number of swarming mosquitoes was significantly higher in the peak phase than in the other phases (start: $n_{swarming}$ = 4.0 ± 0.6 mosquitoes; peak: $n_{swarming}$ = 16.7 ± 2.1; end: $n_{swarming}$ = 6.3 ± 1.4; Table S1). As a result, the relative proportion of swarming mosquitoes to the total number of flying mosquitoes significantly differed across all phases, with the highest proportion observed during the peak phase, and the lowest at the start of swarming (start: $R_{swarming}$ = 26% [9%]; peak: $R_{swarming}$ = 71% [7%]; end: $R_{swarming}$ = 45% [11%]; Table S1).

Flight kinematics of swarming individuals differ from those of mosquitoes flying outside the swarm

Next, we compared the flight kinematics of the swarming mosquitoes with those of mosquitoes flying outside the swarm. The spatial distribution of track densities for all recorded flight tracks highlight three distinct regions (Figure S2): (1) a high-density region above the swarm markers, called the swarming volume, (2) a second high-density region volume along the walls of the flight arena, and (3) a low-density region covering the rest of the flight arena.

The spatial distributions of flight speeds and acceleration magnitudes within the setup (Figures S3 and S4, respectively), show that mosquitoes flying in these three sub-regions also have distinctly different flight kinematics. Within the swarm region, mosquitoes flew with the highest speeds and acceleration magnitudes ($\overline{U}_{swarming}$ = 0.46 ± 0.00 m/s and $\overline{A}_{swarming}$ = 2.48 ± 0.00 m/s^2, respectively). Mosquitoes flying outside the swarming volume flew on average at 57% lower speeds and 67% lower acceleration magnitudes ($\overline{U}_{non\text{-}swarming}$ = 0.20 ± 0.00 m/s and $\overline{A}_{non\text{-}swarming}$ = 0.78 ± 0.00 m/s^2, respectively); near the walls flight, speeds were particularly low (Figure S3).

As mentioned above, the high flight activity observed along the walls of the flight arena corresponds to non-swarming mosquitoes flying repeatedly against the walls as an apparent escape behavior. The swarming volume where mosquito exhibited typical high-speed swarming behavior did not overlap with the regions along the walls where mosquitoes exhibited low-speed flight (Figure S3). This allowed us to separate

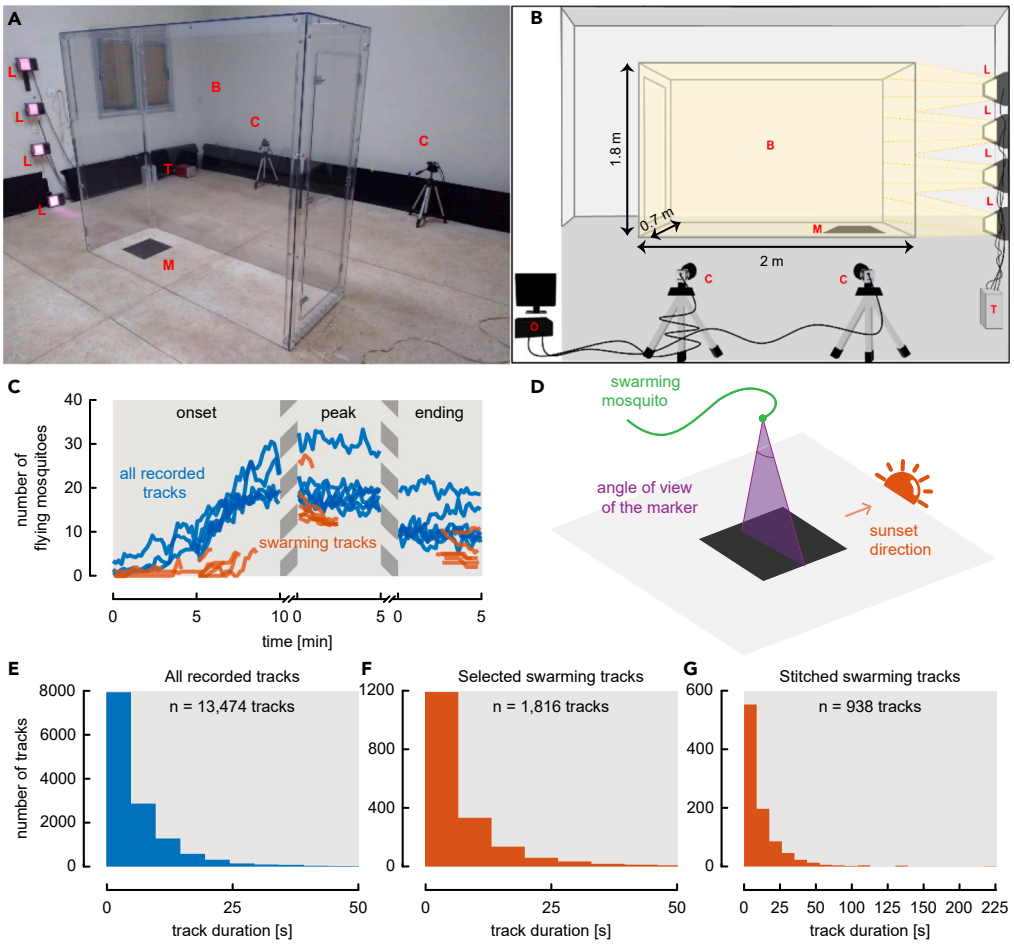

Figure 1. Experimental set-up for mosquito swarming behavior studies

(A and B) Picture and schematic of the set-up, respectively. Capital letters highlight: (B) the Plexiglas box placed in the center of the room; (M) a 40 cm × 40 cm black swarm marker; (C) two synchronized cameras located on (S) the sunset horizon side; (L) the four NIR lamps connected to (T) a controller. Cameras and lamp controller are connected to (O) a computer located outside the room.

(C) Temporal dynamics of flight activity in the entire flight arena and in the swarms (in blue and red, respectively), during the three swarm phrases (start, peak and ending phases), for the six experimental replicates (i.e., swarms).

(D) Schematic of our hypothesis that swarming mosquitoes use the optical angle of the ground marker and sunset direction to position themselves within the swarm.

(E–G) Histograms of track duration of (E) all flight tracks, (F) selected swarming tracks and (G) stitched swarming trajectories of all the recordings.

the swarming mosquitoes from non-swarming mosquitoes, including those interacting with the wall. We focused on these swarming tracks for further analysis.

Flight kinematics of individual swarming mosquitoes differ between the three-dimensional axes while remaining consistent over the swarming duration

As described in previous studies,[17,21,23,24,35,36] the swarming male mosquitoes displayed a stereotypic flight behavior above the black ground marker (Figures 2A–2C, S5A, and S5B). We summarized the flight kinematics of each flight track using the mean ± standard error of the main kinematics parameters (Tables S2 and S3): trajectory location, flight speed, acceleration magnitude (Euclidean norm of the acceleration vector), and the distance to nearest neighbor in the swarm.

We visualized positional kinematics of the swarming flights using the median and quartile distributions for each trajectory (Figures 2D and 2E). These show that most mosquitoes swarms centered above the marker ($\bar{x}$ = 0.00 ± 0.00 m, $\bar{y}$ = 0.00 ± 0.00 m), at an average height of $\bar{z}$ = 0.67 ± 0.01 m (Table S2; Figures 2A–2E). The variation around this mean location due to the swarming flight behavior was significantly smaller in the direction parallel to the sunset horizon than that perpendicular to it ($\bar{\sigma}$ (x) = 0.06 ± 0.00 m and $\bar{\sigma}$ (y) = 0.10 ± 0.00 m, respectively; Table S2 and Figure 2E). The variation in height during the swarming flights was significantly smaller to the variation in both the x and y-direction ($\bar{\sigma}$ (z) = 0.04 ± 0.00 m; Table S2 and Figures 2D and 2E).

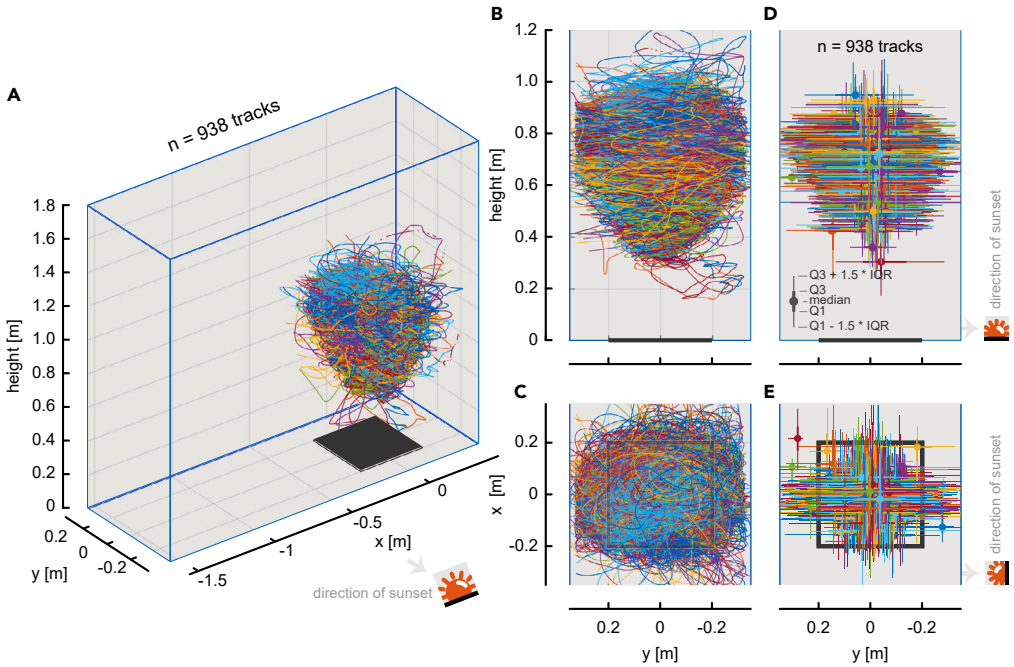

Figure 2. Swarming track locations and flight velocities

(A–C) All selected swarming tracks viewed (A) in three-dimensions, (B) from the side and (C) from the top (n_{track} = 938). (D and E) Side view (D) and top view (E) of the median location and quartiles of each swarming trajectory. The swarm marker is shown in black.

The swarming mosquitoes flew at speeds ranging from 0.24 to 1.28 m/s ($\overline{U}$ = 0.50 ± 0.00 m/s), with acceleration magnitudes ranging from 0.29 to 7.33 m/s^2 ($\overline{A}$ = 2.88 ± 0.02 m/s^2). The average distance to the nearest neighbor was $\overline{d}_{neighbour}$ = 0.11 ± 0.00 m.

The three flight speed components (u,v,w) were significantly different from each other, with the mean vertical speed (w) being the lowest and the mean horizontal speed normal to the sunset horizon (v) the highest (Table S2; Figure S6). Specifically, the mean flight speed normal to the sunset horizon was 1.6 and 4.8 times higher than the flight speed parallel to the sunset horizon and the vertical speed, respectively ($\overline{u}$ = 0.24 ± 0.00 m/s, $\overline{v}$ = 0.38 ± 0.00 m/s and $\overline{w}$ = 0.08 ± 0.00 m/s; Table S2). Similar to the flight speed, the mean acceleration magnitude was highest in the direction normal to the sunset horizon, as it was on average 1.2 and 3.5 times higher than those parallel to the sunset horizon and vertically, respectively ($\overline{A}_x$ = 1.57 ± 0.01 m/s^2, $\overline{A}_y$ = 1.90 ± 0.02 m/s^2, $\overline{A}_z$ = 0.55 ± 0.00 m/s^2; Table S2).

We consequently tested whether the swarming kinematics differed between the three swarming phases (Table S3). Most of the kinematics parameters did not differ significantly among the phases, including the mean and standard deviation of the trajectory locations, the mean speed and mean acceleration magnitude during the swarming flights (Table S3). Only the distance to the nearest neighbor significantly differed across phases: at the peak phase, the mean distance to the nearest neighbor was 1.9 and 1.2 times smaller than at the start and end phases, respectively (start: $\overline{d}_{neighbour}$ = 0.19 ± 0.01 m; peak: $\overline{d}_{neighbour}$ = 0.10 ± 0.00 m; end: $\overline{d}_{neighbour}$ = 0.12 ± 0.00 m; Table S3).

We also analyzed the interaction between the three-dimensional axes and swarming phases (axes × phases interactions; Table S4) to test whether the x, y and z components of flight kinematics parameters varied over the three swarming phases. For all the tested flight kinematics parameters we found no significant axes × phases interaction (Table S4), meaning that the three components (x,y,z) of the swarming kinematics parameters were consistent over the three phases. Furthermore, we found that the tested flight kinematics parameters were consistent among the swarms (Figure S7; Table S5).

Finally, we tested how the swarming kinematics varied with the number of swarming mosquitoes at the peak swarming phase, when the swarm size was relatively constant (Table S3; Figure S8). Again, only the distance to the nearest neighbor varied with the number of swarming mosquitoes, as it decreased with increasing swarm size (Figure S8E). But note the correlation between the number of swarming mosquitoes at the peak swarming phase and the distance to nearest neighbors was weak (r = −0.39).

Size, shape and structure of the complete swarm are stereotypic, non-homogeneous and consistent over the swarming duration

By combining the individual flight tracks of all swarming mosquitoes, we quantified the emerging kinematics of the swarm as a whole, for the three swarming phases separately (Figure 3), for the six separate swarms (Figure S9), and for all swarming mosquitoes combined (Figures 4 and 5). For each case, we visualized the swarming kinematics using the spatial distribution of normalized swarming density (Figures 3 and S9). We observed that the size, shape and structure of swarms were consistent over the phases and across the six swarms (Figures 3 and S9, respectively). This similarity, in addition to the consistency in the mosquito flight kinematics across phases and swarms, allowed us to combine all

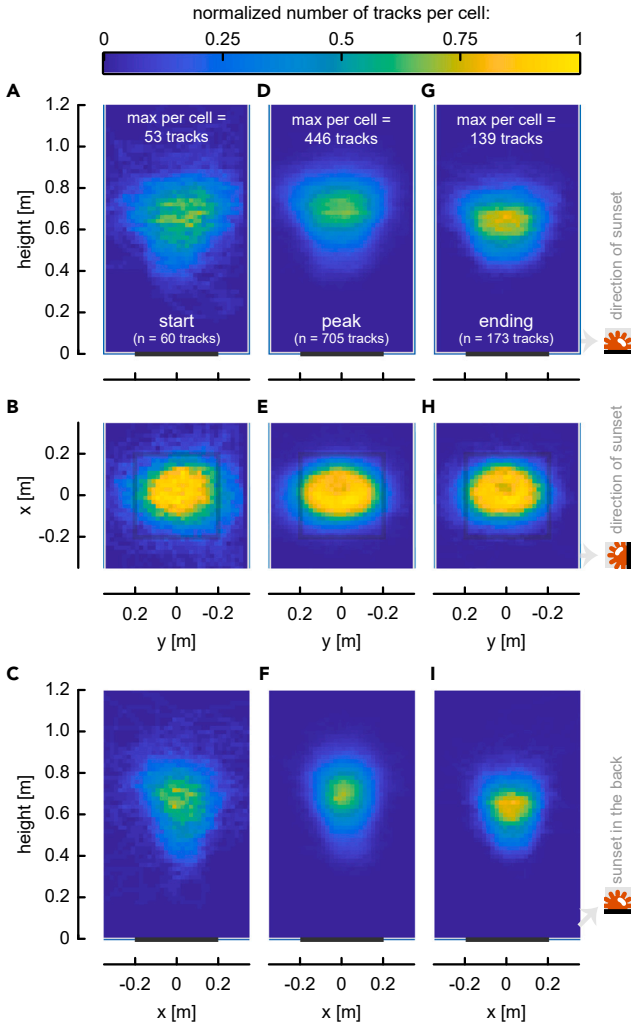

Figure 3. Swarm shape and spatial distribution of swarming track density at the three swarming phases

The spatial distribution of the number of swarming tracks per cell recorded at (A–C) the start, (D–F) peak and (G–I) ending phases of swarming activity. The number of tracks for each swarm has been normalized by the maximum number of tracks computed per cell in order to facilitate comparison between swarming phases. The swarm marker is shown as a black line or square.

swarming data into a large dataset in order to reconstruct the average swarm, with which we subsequently worked (Figures 4 and 5). Note that such pooling was necessary for these consecutive analyses, due to the stochasticity of swarming and the relatively low number of individual mosquitoes recorded per swarm.

The observed swarm is shaped as a flattened elliptical cone, because it is wider at the top (~0.5 m) than at the bottom (~0.2 m) (Figures 2A–2E and 4A–4C), and it is slightly stretched horizontally in the direction of the sunset horizon (*y* axis). The center of the swarm is positioned straight above the visual ground marker, and the top and bottom of the swarm were located at a height of approximately 0.95 m and 0.35 m, respectively (Figures 2A and 4A–4C).

The density of swarming flight points and tracks was higher in the middle of the swarms (Figures 4D–4I) gradually decreasing toward top, bottom and side boundaries. Particularly, at the top and bottom regions, densities were approximately three times lower than in the middle section (Figures 4D and 4G). Nevertheless, mosquitoes that went in the lower half of the swarm stayed significantly longer in this region with durations approximately twice of those in the upper section (Figures 4J–4L). In contrast to the density of swarming flight tracks, the distance to the nearest neighbors was the lowest in the middle of the swarm with mosquitoes flying around two times as close to each other in the middle of the swarm than at boundaries (Figures 5A–5C).

Examining the spatial distributions of the flight kinematics parameters reveals that swarming mosquitoes were flying 1.25 times faster in the top half of the swarm compared to the lower section (Figures 5D–5F). However, the acceleration magnitudes were the highest at the boundaries of the swarm, gradually reducing to nearly zero along the central axis of the swarm $y = 0$ m (Figures 5G–5I).

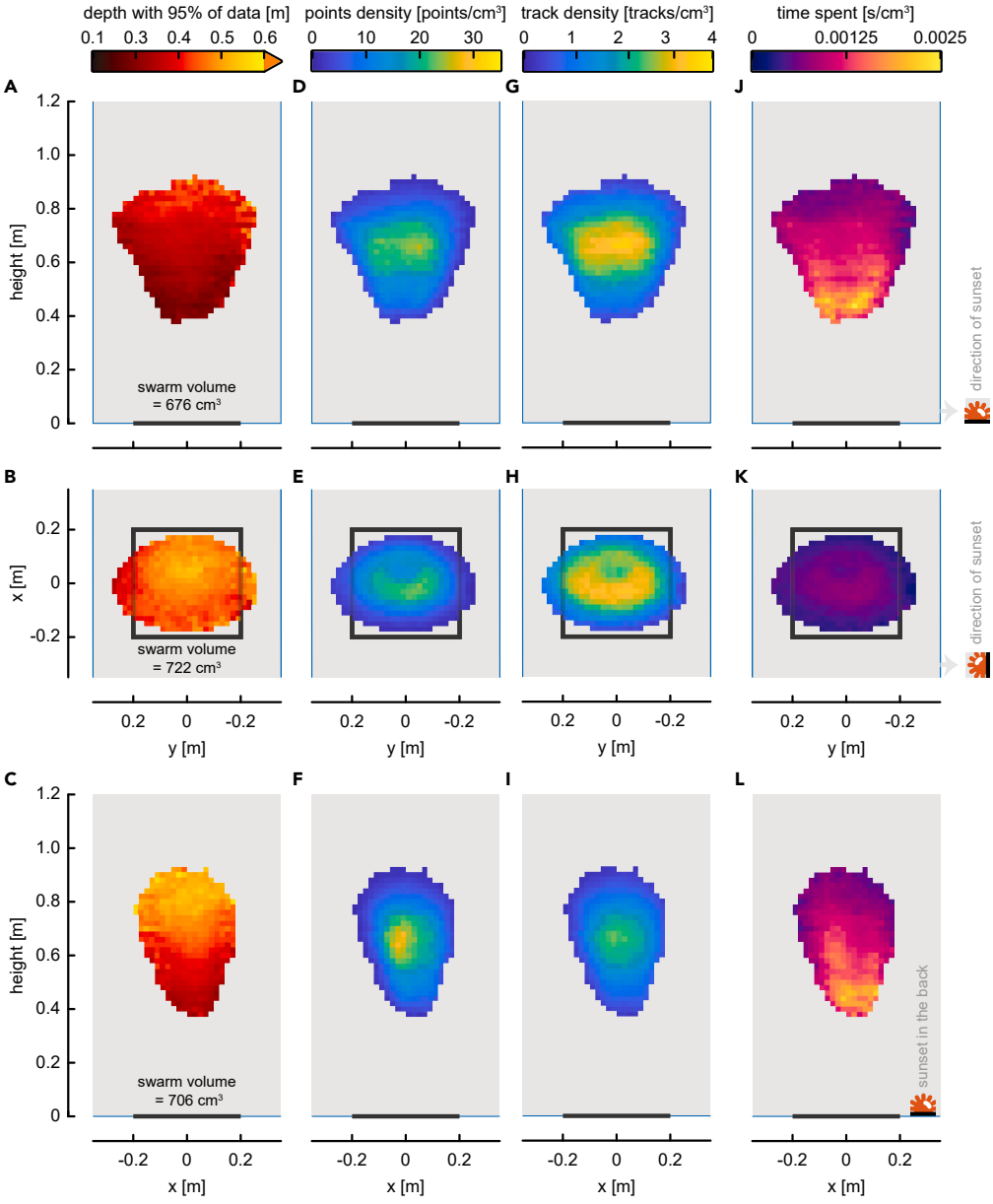

Figure 4. Swarm shape and structure

(A–C) Spatial distributions of the depth of each sub-volume comprising of 95% of the three-dimensional tracking data. These heatmaps describe the three-dimensional shape of the swarms.

(D–I) Spatial distributions of the point density (D–F) and the track density (G–I) per cm^3.

(J–L) Spatial distribution of the mean time spends in each cm^3 within the swarm. Cell with less than an average of one track per swarm and per recording (i.e., 6 swarms × 3 recordings = 18) were filtered out. The top, middle and bottom row show the swarm viewed from parallel to the sunset horizon, the top and normal to the sunset horizon, respectively (see sunset symbol). The swarm marker is shown as a black line or square.

Mosquito swarming behavior can be modeled based on visual perception of the swarm marker

After finding that the swarm kinematics were highly consistent across the three swarming phases and the six swarms, we used the average swarm location, size and shape to develop, test and validate our sensory-cue informed model (Figures 6 and S10). We first developed a mathematical representation of the average swarm reconstructed from our experimental data (Figures 6B and 6D–6F). This consists of the previously described flattened elliptical cone, of which the short and long primary ellipse axes increase in size with height (Figures 6B, S10A, and S10D). The long axis is oriented normal to the sunset horizon, and the short axis is oriented parallel to it.

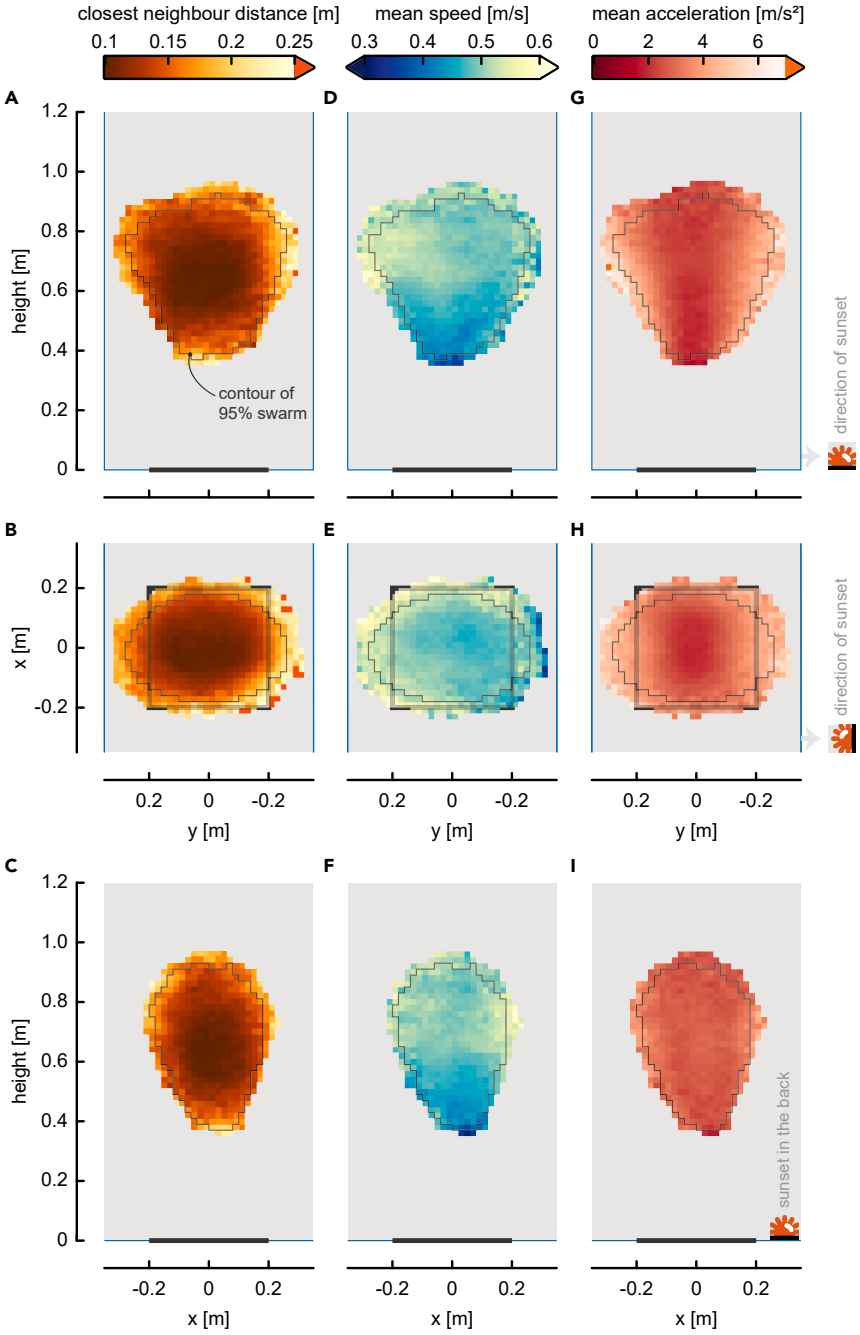

Figure 5. Spatial distribution of swarming flight kinematics

(A–C) Spatial distribution of the mean distance to the closest neighbor.

(D–I) Spatial distribution of the mean flight speed (D–F) and mean acceleration magnitude (G–I), for mosquitoes swarming in each 2 cm × 2 cm cell. The top, middle and bottom row show the swarm viewed from parallel to the sunset horizon, the top and normal to the sunset horizon respectively (see sunset symbol). The swarm marker is shown as a black line or square.

Our model assumes that mosquitoes within this swarm volume use visual cues, particularly optical angle of the ground marker to display the swarming behavior (Figures 6A, S11B, and S11C). We therefore calculated the optical angles that mosquitoes would perceive of the marker throughout the complete swarming area (Figures 6D–6F). Because the swarm circumference is elliptical, we calculated the optical angle of the marker along the *x* and *y* axis separately (α and β, respectively; Figures S10B and S10C). Optical angles of an object are inversely proportional to the distance from that object, and thus the optical marker angles decrease with increasing height above the marker, but also when moving horizontally from the middle of the marker to the edges.

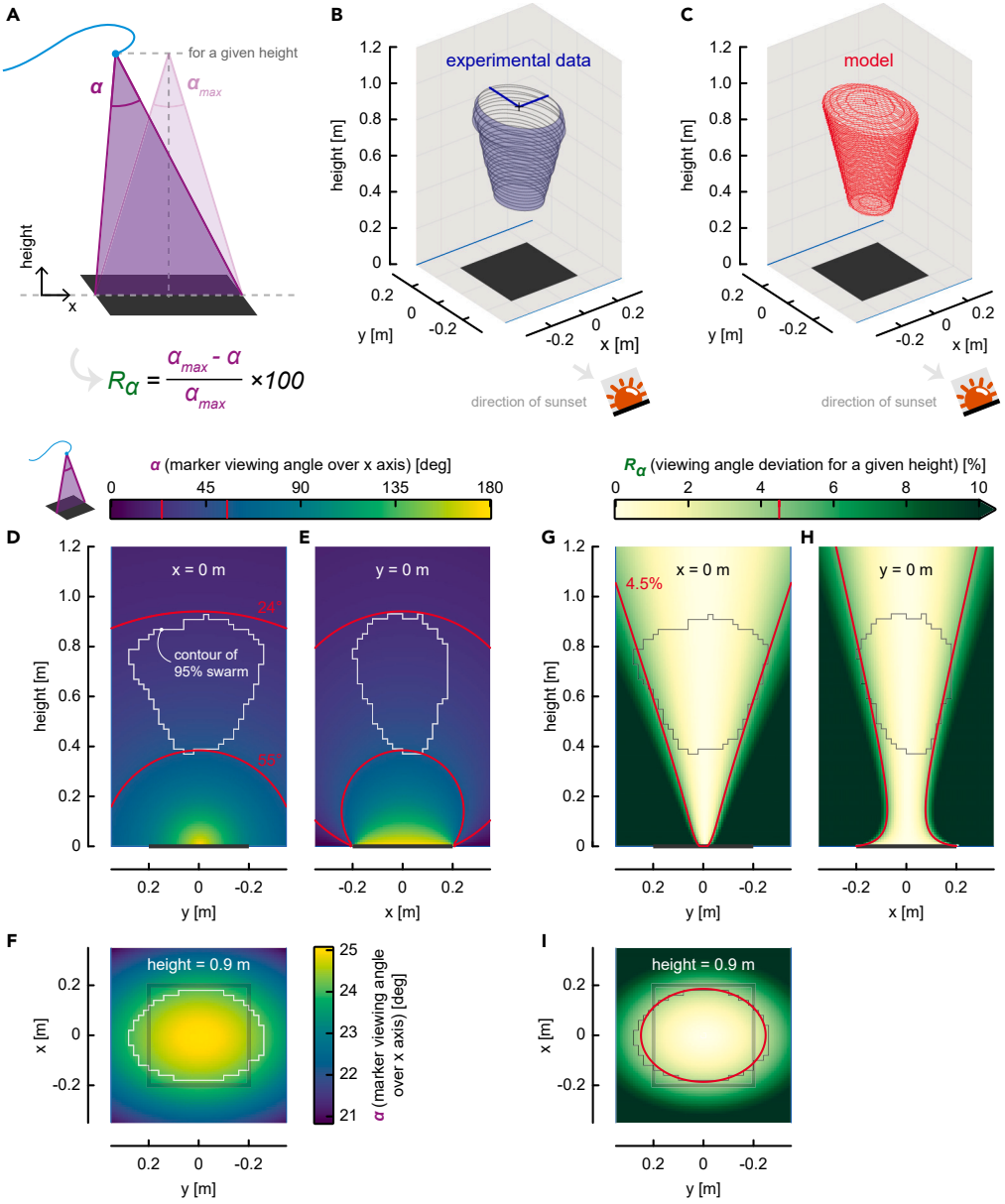

Figure 6. Modeling the marker viewing angle and the three-dimensional swarm shape

(A) Schematic showing how the viewing angle of the marker α and the viewing angle deviation R_α are defined at a given height.

(B and C) The three-dimensional shape of the swarm based on experimental data (B), and on our mosquito vision-informed model (C). Both consist of a set of ellipses, based on (B) the experimental swarm radiuses along the *x*-axis and *y* axis, and (C) on the model parameters shown in (D–I).

(D–F) The marker viewing angle along the *x*-axis (α) throughout 3D space, viewed from parallel to the sunset horizon, normal to the sunset horizon and top, respectively. The red and white lines show viewing angle iso-lines (α = 24° and α = 56°) and the swarm contour, respectively.

(G–I) The percentage difference R_α between the maximum viewing angle over *x*-axis and current viewing angle for a given height, viewed from parallel to the sunset horizon, normal to the sunset horizon and top, respectively. The red and gray lines show iso-lines of R_α = 4.5% and the swarm contour, respectively. The swarm marker is shown as a black line or square.

We then used these optical data in combination with the mathematical representation of the average swarm to estimate how swarming mosquitoes could use their visual perception of the ground marker to display the swarming behavior. We defined the top and bottom boundaries of the swarm based on absolute optical angle values (Figures 6D and 6E), and the cone-like side edges of the swarm based on the change in optical angle (optic flow cues).

We first tested how the optical angles of the marker in the directions parallel and normal to the sunset horizon captured the observed elliptical swarm shape (Figures S10B and S10C). For this, we calculated both optical marker angle parameters α and β, at the swarm edge

along both the short and long ellipse axes (*x* and *y*-directions). In this way, we computed two values of both α and β for a range of equidistantly spaced 29 heights. Results showed that, for any given height, the α optical angles computed at the edge of the swarm are the same along both ellipse swarm axes (Figure S10B), but they differ for the β optical angles (Figure S10C). Thus, at any given height α was found to be constant along the complete elliptical contour of the swarm, while β was not. This suggests that swarm shape is linked to the optical angle parallel to the sunset horizon α, and that swarming mosquitoes would use this angle to continue flying within the elliptical circumference of the swarm.

Secondly, we tested what might cause the increase in swarm circumference with increasing height. We hypothesized that swarming mosquitoes use the change in optical angle as cue to stay inside the swarm edge and move back toward the middle. To test this, we determined at various heights the percentage decrease in the α and β optical marker angles when moving from the swarm center toward the edge, along both ellipse axes (Figures S10E and S10F). The relative optical angle change along the *x*-axis is defined as $R_\alpha=(\alpha_{max}-\alpha)/\alpha_{max}\times100\%$, where α_{max} is the maximum optical angle at the center of the swarm in the *x*-direction. The relative optical angle R_α at the edge in the *x*-direction turned out to be consistently 4.5% of the maximum angle, along both ellipse axes and at all swarm heights (Figure S10E). In fact, the 4.5% threshold at a given height exactly produces the elliptical circumference observed in the swarming experiments (Figures 6F–6I). In contrast, the relative optical angle R_β at the edge in the *y*-direction differed between both ellipse axes, as it was consistently 2.5 and 8.0 along the *x* and *y* axis, respectively, at all swarm heights (Figure S10F). This further supports the notion that swarming mosquitoes use the optical angle in the *x*-direction (α) to fly within the circumference of the swarm.

Because swarming mosquitoes apparently use the optical angle of the marker in the *x*-direction (α) to control their horizontal position within the swarm, we determined the optical angle α at the bottom and top of the swarm (Figures 6D and 6E). It appears that at the bottom and top of the swarm mosquitoes experienced an α optical angle of the marker of 55° and 24°, respectively. These angles could thus be used by mosquitoes as thresholds to conform to the swarm height distribution. The resulting modeled swarm shape and size captured the experimentally measured swarm well (Figures 6B–6I).

DISCUSSION

Mosquito flight activity differs across the swarming phases

By combining videography-based experiments with modeling, we studied the flight kinematics of *A. coluzzii* male mosquitoes during simulated sunset and how their collective flights result in emergent swarming behavior. At the start of sunset, resting males first started to fly throughout the complete flight arena. Then, the swarm was initiated by a male performing repeated stereotypic flights over the visual ground marker. Within the following minutes, it was sequentially joined by other mosquitoes, resulting in the development of a swarm. The number of swarming males increased over time to reach a peak swarming phase approximately 10 min after the start. The swarm remained relatively stable for approximately 10 min, after which the swarm size gradually decreased, and swarming ended approximately 30 min after it started. The mosquitoes that stopped swarming often kept flying. This post-swarming flight activity is distinctly different from the pre-swarming activity, as here the male mosquitoes repeatedly fly against the inner walls of the arena.

On the assumption that both male and female mosquitoes use swarm markers to find and join mating sites,[20,21,23] we suggest that at the start of sunset, the non-swarming flight continues until the mosquito find an appropriate visual ground marker. Then, the male mosquito initiates a stereotypic swarming flight pattern above the marker until it detects a potential mate. The presence of swarming male mosquitoes at a site may also visually attract other males to the swarm, but this remains to be proven. The post-swarming flight activity near the walls of the arena suggests that these mosquitoes exhibit a dispersal flight behavior, possibly seeking for a food source after their energetically costly swarming flights.[37,38]

During our experiments, we simulated sunset light conditions by slowly reducing ceiling light intensity and providing a sunset horizon. The increase in flight activity and the start of swarming were both triggered by the sunset simulation, although the circadian clock also plays a key role in the process.[39–41] After the initial sunset simulation, light intensity in the experimental room were kept constant. Thus, light conditions remained unchanged from 2 to 3 min before the first male started swarming until after the ending of swarming. Because swarm ending occurred approximately 30 min after swarm initiation, swarm ending could not have been triggered by changes in light conditions. Swarming flight behavior has an exceptionally high energetic cost,[37,38] suggesting that the male mosquitoes stopped swarming when a threshold in their energy reserve was reached.

The high energy cost of swarming could be explained by the shift from an exploratory flight behavior with both low flight speed and accelerations to a swarming flight behavior with higher flight speeds and rapid accelerations. Further investigations on the pre-swarming and post-swarming random flight behaviors could provide information on the mating site searching behavior and other relevant behaviors that occur around swarming.

The post-swarming flight activity near the flight arena walls could be the result of an escape-like flight behavior or straight flight of mosquitoes in search for a sugar meal to refuel their reserves. If energy reserves limit the duration that a male mosquito is able to remain swarming, then presence in a swarm is a good signal of male fitness for the female seeking a mate.[42] Swarming duration could thus equally be used by researchers to assess the potential fitness of laboratory male mosquitoes used in mosquito release programs.[21,23,40,43]

The location and stereotypic shape of the swarm are governed by the viewing angle of the swarm marker and the sunset horizon

As expected in *A. coluzzii* mosquitoes, males located their swarms above the visual ground marker. This behavior has been previously reported and discussed as the primary premating barrier governing the swarm spatial segregation and the reproductive isolation in *A. gambiae s.l.*[18,21,44]

The swarm was consistently located right above the marker at an average height of 0.67 m and was shaped like an upside-down elliptical flattened cone. The swarming mosquitoes flew above the marker with optical viewing angles of the marker ranging from 24° to 55°. These values would be the minimum and maximum thresholds in our experimental conditions to set the height range of the swarm above the marker. If true, a larger marker should induce higher and wider swarms, which was reported by Poda et al.[21] This would suggest that these features are probably governed by environmental visual cues, but the consistency of viewing angle range with different marker sizes needs to be confirmed in further studies.

As both sexes use the marker to join the species-specific mating site,[17,21,24] the range of viewing angle used by both males and females need to be consistent and species-specific to bring sexes together. This relation of the swarm to the marker was also closely studied in other mosquito species. In laboratory conditions, *Culex pipiens quinquefasciatus* males formed swarms above a 26 cm square marker where the marker viewing angle ranged from 40° to 90°.[24] However, the height of swarms may differ locally[45] and consequently, the marker viewing angle could depend on local adaptations.

The upside-down cone shape of the swarm can be explained by the fact that at a given height, males did not deviate in the horizontal plane by more than 4.5% from the maximum viewing angle parallel to the sunset horizon. As a result, the horizontal flight amplitude that allows staying within the swarm volume increases with height. Our mathematical model is based on the optical angle of the marker and predicted well the location and shape of the swarm found from the experimental data, assuming that these would be primarily based on optical metrics of the swarm marker and the orientation of the swarming mosquitoes to the sunset horizon.

Our sensory-system informed model, although fitted on our experimental results, shows that the most important swarm shape characteristics can be reproduced well based on a small set of visual cues of the swarm marker and sunset. This provides the basis for testing how mosquito swarming emerges from a combination of intrinsic flight behavior and external cues. For such follow-up research, it would be useful to develop richer behavioral models, and perform swarming experiments in large cages in semi-field conditions, with variable swarm marker sizes and shapes, natural sunset, and with different mosquito strains and species.

Swarm shapes depend on both intrinsic behavior and extrinsic external cues

In previous studies, various swarm shapes have been observed for mosquitoes and midges swarming in both lab and field conditions.[17,21,24,26,32,46,47] All these emergent swarm shapes are the result of a complex interplay between intrinsic behavior of the swarming insect and extrinsic external cues. Therefore, these differences in swarm shape are likely due to differences in the animals used for the experiment (intrinsic variations), and variations in the experimental conditions (extrinsic variations).

Arguably, the most important variations in extrinsic environmental cues between different studies include the characteristics of the experimental setup, the visual marker, and the surrounding skyline and sunset.[26,48] Also, wind speed and direction influence swarm characteristics,[17,26,49] but wind was absent in our lab-based study.

The intrinsic behavior varies strongly between mosquito species,[21] but might also differ between mosquitoes strains.[45] Hereby, wild type mosquitoes are expected to produce the most natural swarm behavior. Because our mosquito line were only two generations separated from wild type (F2), we can assume that the intrinsic swarm behavior of our mosquitoes is close to natural.

We show that our male mosquitoes produce, in the vertical plane, a cone-shaped swarm. In contrast, Cavagna et al.[32] describes their male swarms as cylindrical or barrel-shaped.[32] For their experiments, Cavagna et al.[32] used a strain of *A. gambiae* that has been lab-reared since 1975. This different reported between the swarms of Cavagna et al. and our F2 *A. coluzzii* swarms might be due to differences in experimental conditions and/or mosquito strains.

In the horizontal plane, our mosquitoes produce an elliptical swarm shape, which was similar to the elliptical shapes found in swarms of other *Anopheles* mosquitoes,[17] as well as in midge swarms.[46] This suggests that also this aspect of swarm kinematics is well preserver, potentially even beyond the *A. gambiae* complex. Note that Cavagna et al. instead reported circularly-shaped swarms, instead of an elliptical one.[32] The cause of this difference might be due to differences in experimental conditions.

The elliptical cone-shaped swarm outline might result from differential flight patterns

Within the swarm volume, mosquitoes flew mainly in the horizontal plane with variable flight speeds and acceleration magnitudes. Both horizontal flight speeds and acceleration magnitude were higher in the direction of the artificial sunset horizon (*y* axis) than parallel to it (*x*-axis) (Table S2). This differential flight patterns along the *x*-axis and *y* axis might be the cause of the elliptical swarm shape with the minor and major ellipse axes aligning with *x*-axis and *y* axis, respectively.

The differential flight speeds pattern could be due to the location of the marker in the flight arena and/or to the rectangular shape of the flight arena. However, the widest side of the flight arena was parallel to the sunset horizon (*x*-axis), which is the direction in which the swarm was narrowest. Furthermore, this flight pattern has also been reported in natural swarms of *A. gambiae s.l.* in the field.[30] Here, swarming individuals were primarily flying in the horizontal plane, with the longest fight distances and highest flight speeds in east–west direction (normal to the sunset horizon).[30]

The above-mentioned similarities between our swarms and those of other studies[30] suggest that our observed swarm characteristics are most likely the result of a behavioral orientation relative to the sunset rather than a set-up bias. This is further supported by our model that suggests that our swarming mosquitoes consistently use the optical marker angle parallel to the sunset horizon for positioning themselves above the marker. Orienting toward the sunset would not only allow swarming mosquitoes to robustly assess this optical angle of the marker, but also generate a good viewing of the surrounding and consequently of potential mates entering the swarm.

In contrast to the primarily horizontal flight pattern of swarming *A. gambiae s.l.*, other mosquito species such as *Cx. pipiens quinquefasciatus* exhibits mainly vertical flight movements in swarms.[24] This suggests that our results could be specific to the species of the *A. gambiae* complex.[21,30,32]

The swarm structure is non-homogeneous and flight kinematics vary throughout the swarm volume

Our recordings revealed a higher density of flight tracks in the middle of the swarm resulting in shorter distances between individuals in this region, something that was also reported from natural swarms of *A. gambiae s.l.*[26,30,31] According to Manoukis et al.,[26] this location could confer an advantage to the males as it allows a quicker access to any part of the swarm periphery and thus a quicker access to females if they randomly enter swarms. In addition, once in the swarm, females may simply be more likely to pass through the middle of the swarm, making this location a hotspot for mating.

Alternatively, this location in the swarm could simply be a by-product of mosquito perception of the marker. Our results provide further support for the latter hypothesis. Indeed, if swarming males must fly directly above the marker without losing eye-contact with it and have to fly within a given range of marker viewing angle, which probably contains an optimal value, a pattern such as the one observed could emerge. The middle of the swarm could be the region of the optimal marker viewing angle. If this hypothesis is true, the same swarming flight pattern will be observed in any species using a fixed visual landmark to define the location and volume of the swarm.

Another hotspot could be the lower half of the swarm, as we found that males spent more time in this area. Butail et al.[30] reported that females were observed predominantly in this area just before the copula. This location in the swarm could also simply be a by-product of the perception of the marker by both the male and female mosquitoes.

The spatial distributions of flight kinematics parameters showed that swarming mosquitoes were flying faster in the top half of the swarm, and the flight acceleration magnitudes were higher at the boundaries and close to zero along the central axis of the swarm. This is probably due to the swarm shape and its fixed volume, both governed by the mosquito perception of the marker. First, swarming individuals were mainly flying horizontally and located in the area above the marker by flying at relatively constant speeds in the center of the swarm and rapidly turning at the swarm edges, leading to high acceleration magnitude. Secondly, the upside-down cone shape of the swarm provides large horizontal flight amplitudes in the top region of the swarm, allowing faster flights in this region. This could explain the fact that mosquitoes spent less time in this region because of the high energetic cost of the swarming flight.[37,38]

Swarm structure and flight kinematics of individual swarming mosquitoes are consistent over the swarming period

Except for the number of individuals in the swarm and the distance to the closest neighbor, the characteristics of the swarm as a whole did not significantly change between the start, peak and ending phases of swarming activity. The location, dimensions and shape of the swarm as well as the flight pattern of the swarming individuals were consistent over the three swarming periods, regardless of the number of individuals in the swarm. This has also been reported in *Cx. pipiens pallens*,[25] and supports the hypothesis that the location, volume, and shape of the swarm are defined by the visual characteristics of the marker.[21,24,26,48] However, Feugère et al.[23] showed differences between *A. coluzzii* and *A. gambiae s.s.* in radius of field swarms as a function of number of males, where *A. gambiae s.s.* showed a positive effect of number of swarming males over the swarm radius. Previous research on swarming midges showed that the distance to the nearest neighbor also depends on the number of swarming individuals, and that there is a minimal threshold distance between swarming individuals.[46] Whatever the cause, the swarming space, which would be defined by the marker size, cannot contain an infinite number of individuals due to a saturation effect in the swarm size.[21] Each male in a swarm would need a given airspace to produce the stereotyped swarming flight.

While the volume of the swarm remained consistent, the number of individuals within the swarm varied over the swarming period. This resulted in a variation in the distance to the nearest neighbor, which was shortest during the peak phase when swarm density was highest. Furthermore, within the peak swarming phase, the distance to the nearest neighbor decreased with increasing number of individuals in the swarm, although the correlation was weak. This weak correlation might be due to the relatively small range in number of the swarming mosquitoes during the peak swarming phase, resulting in limited statistical power for testing this effect. Regardless, swarming individuals need to keep some minimal distance from each other to display their stereotypic swarming flights while avoiding collusions; hence, the saturation effect in swarm size reported by Poda et al.[21]

Regarding the mosquito flight kinematics, neither the flight speed nor acceleration magnitude changed significantly between the three swarming phases. This suggest that male mosquitoes in the swarms have the same ability to mate over the swarming period, and mating can successfully occur within the swarm at any time of the swarming period.

Mosquito swarming placed in a broader context

Our experimental set-up allowed three-dimensional recording of the flight activity of *A. coluzzii* males at the start, peak and ending phase of swarming. Data analysis provided relevant quantitative information on the spatial and temporal dynamics of the swarm characteristics, mosquito flight kinematics and their relationship with the swarm marker. All these metrics were highly consistent across the six swarms and the three swarming phases suggesting the repeatability of the experiments, and the consistency of the swarming individual behavior over the swarming period, respectively. However, the swarm had a non-homogeneous structure and a differential spatial distribution of the swarming flight kinematics, most likely governed by the mosquito perception of the swarm marker.

These findings may help to explain mechanisms underlying speciation and diversification within the *A. gambiae* complex as any single significant change in the swarming flight behavior or in the utilization of the swarm marker could lead to divergence in a mosquito population

and promote speciation. Similar works within the *A. gambiae* complex may provide information on which of the studied metrics differ between the species and thus can be involved in speciation or conspecific recognition.

In the field of vector control, such changes may be induced during colonization or genetic modification of mosquitoes used in release programs potentially compromising their competitiveness and mating success in the field. Therefore, these metrics may be used to assess impact of colonization or genetic modifications on mosquito swarming behavior, or to gauge competitiveness of produced males.

Limitations of the study

The study was carried out in laboratory settings, under artificial environmental conditions, simulated sunset, and with a limited number of mosquitoes. These aspects could influence mosquito flight activity, before, during and after the swarming period. Specifically, artificial sunset light, while triggering swarming flight in mosquitoes, could influence the time of the onset of flight and swarming activities as well as the swarming duration. Although it has been reported that mosquitoes do not seem to be disturbed by NIR lights,[50] the use of this unnatural light may still influence mosquito swarming behaviors. The enclosed flight arena could influence flight behavior by limiting mosquito flight maneuvers, especially during the pre-swarming and post-swarming periods. The swarm shape and flight kinematics recorded in our set-up in laboratory conditions and in absence of airflow might differ from those that would be recorded in the field in the presence of wind, although similar observations have been reported from field studies.[26,30,31] The limited number of mosquitoes used in the experiments resulted in relatively small swarms. Individuals flying in large swarms might exhibit different flight kinematics to those recorded in our experiments.

Additionally, as one of the main limitations of video tracking data of mosquito swarm trajectories,[22,30] our tracking system was not able to reconstitute the whole flight trajectory of each mosquito in the flight arena. This limits the information on individual movements inside and outside the swarms. As a result, some flight kinematics parameters, such as time spent in the swarm or in a sub-volume of the swarm, could be underestimated. Further studies could address these experimental limitations by comparing swarming kinematics in our laboratory experiments with those of swarms in semi-field or field conditions. Such experiments require the development of three-dimensional tracking systems that can operate reliably in semi-field or field conditions.

Our study focusses on the emergent kinematics of male mosquito swarms as a whole, by analyzing the combined flight kinematics of subsets of in total 938 swarming mosquitoes within six swarms. And thus, we did not analyze the flight kinematics of the individual mosquitoes in detail. As described in previous studies, the flight patterns of individual swarming mosquitoes are highly complex,[24,46,47] something that our analysis based on the swarm kinematics as a whole does not capture. Future analyses, based on the detailed flight pattern of individual mosquitoes, are needed to further investigate how the combined flights of individual mosquitoes result in the observed emergent swarm dynamics.

Furthermore, we based a large part of our analyses on the combined dataset of all 938 swarming flight tracks within all six swarms. This pooling of data was necessary due to the stochasticity of swarming and the relatively low number of individual mosquitoes recorded per swarm. Such analysis thus reconstructs the swarm characteristics of a generic swarm of male malaria mosquitoes in the here-tested lab conditions, and ignores variations in swarming characteristics between swarms and with time.

We used our relatively simple sensory-system inspired model to test what visual cues might be used by swarming male mosquitoes for staying within the swarm perimeter. Such simplified model does not allow us to model and identify the detailed sensory-motor kinematics that these swarming mosquitoes exhibit, but this is outside the scope of the current study. To enable such analysis, one would need to develop a more complex model such as an agent-based one.[51]

RESOURCE AVAILABILITY

Lead contact

All requests for additional information and resources should be directed to Bèwadéyir Serge Poda (sergepoda71@yahoo.fr), Institut de Recherche en Sciences de la Santé (IRSS), Bobo-Dioulasso, Burkina Faso.

Materials availability

This study did not generate new unique reagents.

Data and code availability

- Data reported in this paper is publicly available in the DRYAD repository. The link is listed in the key resources table.
- All original MATLAB and R codes is publicly available in the DRYAD repository. The link is listed in the key resources table.
- Additional data and additional information required to reuse and reanalyze the data reported in this paper is available from the lead contact upon request.

ACKNOWLEDGMENTS

We thank Somda Stéphane, Sougué Emmanuel, Guinko Nourou, Coulibaly Valérie and Bandaogo Abdoul Malik for mosquito rearing. We are grateful to Wageningen University and Research for training and material support during the data analysis and drafting of the manuscript. This work was funded by an Agence National de la Recherche grant (ANR-15-CE35-0001-01) awarded to O.R., and a grant from the Human Frontier Science Program (RGP0044/2021) to F.T.M. and A.D.; B.S.P. received financial supports through a doctoral fellowship from the Institut de Recherche pour le Développement (France), a doctoral fellowship from

the government of Burkina Faso (Burkina Faso) and a postdoctoral fellowship from the Wageningen Graduate School of Wageningen University (The Netherlands).

AUTHOR CONTRIBUTIONS

B.S.P., O.R., M.F., and P.M. installed and calibrated the video tracking system. B.S.P. and O.R. conceived the experimental design. B.S.P., C.N., and D.F.S.H. performed data collection. B.S.P., A.C., and F.T.M. performed data analyses. B.S.P. and A.C. drafted the figures. B.S.P., M.F., and L.F. performed data analyses on a preliminary experiment. B.S.P. drafted the manuscript and A.C., F.T.M., O.R., and L.F. critically revised the manuscript. All authors revised the manuscript, gave final approval for publication and are accountable for the work performed therein.

DECLARATION OF INTERESTS

The authors declare no competing interests.

STAR★METHODS

Detailed methods are provided in the online version of this paper and include the following:

- KEY RESOURCES TABLE
- EXPERIMENTAL MODEL AND STUDY PARTICIPANT DETAILS
  - Animals
- METHOD DETAILS
  - Video tracking system
  - Laboratory set-up
- EXPERIMENTAL DESIGN FOR MOSQUITO FLIGHT RECORDING
- QUANTIFICATION AND STATISTICAL ANALYSIS
  - Experimental data processing
  - Characterising the flight kinematics of individual swarming mosquitoes
  - Characterising and visualising the kinematics of the complete swarm
  - Modeling mosquito swarming behavior
- STATISTICAL ANALYSES OF EXPERIMENTAL DATA

SUPPLEMENTAL INFORMATION

Supplemental information can be found online at https://doi.org/10.1016/j.isci.2024.111164.

Received: April 16, 2024
Revised: July 2, 2024
Accepted: October 9, 2024
Published: October 11, 2024

REFERENCES

1. World Health Organization (2023). World Malaria Report (World Health Organization).
2. World Health Organization (2018). World Malaria Report (World Health Organization).
3. Bhatt, S., Weiss, D.J., Cameron, E., Bisanzio, D., Mappin, B., Dalrymple, U., Battle, K., Moyes, C.L., Henry, A., Eckhoff, P.A., et al. (2015). The effect of malaria control on *Plasmodium falciparum* in Africa between 2000 and 2015. Nature *526*, 207–211. https://doi.org/10.1038/nature15535.
4. Toé, K.H., Jones, C.M., N'Fale, S., Ismail, H.M., Dabiré, R.K., and Ranson, H. (2014). Increased pyrethroid resistance in malaria vectors and decreased bed net effectiveness, Burkina Faso. Emerg. Infect. Dis. *20*, 1691–1696. https://doi.org/10.3201/eid2010.140619.
5. Ranson, H., and Lissenden, N. (2016). Insecticide resistance in African *Anopheles* mosquitoes: a worsening situation that needs urgent action to maintain malaria control. Trends Parasitol. *32*, 187–196. https://doi.org/10.1016/j.pt.2015.11.010.
6. Hemingway, J., Beaty, B.J., Rowland, M., Scott, T.W., and Sharp, B.L. (2006). The innovative vector control consortium: improved control of mosquito-borne diseases. Trends Parasitol. *22*, 308–312. https://doi.org/10.1016/j.pt.2006.05.003.
7. Beier, J.C., Keating, J., Githure, J.I., Macdonald, M.B., Impoinvil, D.E., and Novak, R.J. (2008). Integrated vector management for malaria control. Malar. J. *7*, S4. https://doi.org/10.1186/1475-2875-7-S1-S4.
8. World Health Organization (2012). Global Plan Management Resistance for Insecticide in Malaria Vectors (World Health Organization).
9. Poda, B.S., Guissou, E., Maïga, H., Bimbile-somda, S.N., Gilles, J., Rayaisse, J.B., Lefèvre, T., Roux, O., and Dabiré, R.K. (2018). Impact of irradiation on the reproductive traits of field and laboratory *An. arabiensis* mosquitoes. Parasites and Vectors *11*, 641. https://doi.org/10.1186/s13071-018-3228-3.
10. Helinski, M.E.H., Hassan, M.M., El-Motasim, W.M., Malcolm, C.A., Knols, B.G.J., and El-Sayed, B. (2008). Towards a sterile insect technique field release of *Anopheles arabiensis* mosquitoes in Sudan: Irradiation, transportation, and field cage experimentation. Malar. J. *7*, 65. https://doi.org/10.1186/1475-2875-7-65.
11. Nolan, T., Papathanos, P., Windbichler, N., Magnusson, K., Benton, J., Catteruccia, F., and Crisanti, A. (2011). Developing transgenic *Anopheles* mosquitoes for the sterile insect technique. Genetica *139*, 33–39. https://doi.org/10.1007/s10709-010-9482-8.
12. Yao, F.A., Millogo, A.A., Epopa, P.S., North, A., Noulin, F., Dao, K., Drabo, M., Guissou, C., Kekele, S., Namountougou, M., et al. (2022). Mark-release-recapture experiment in Burkina Faso demonstrates reduced fitness and dispersal of genetically-modified sterile malaria mosquitoes. Nat. Commun. *13*, 796. https://doi.org/10.1038/s41467-022-28419-0.
13. Caragata, E.P., Dutra, H.L.C., and Moreira, L.A. (2016). Exploiting Intimate Relationships: Controlling Mosquito-Transmitted Disease with *Wolbachia*. Trends Parasitol. *32*, 207–218. https://doi.org/10.1016/j.pt.2015.10.011.
14. Hughes, G.L., Koga, R., Xue, P., Fukatsu, T., and Rasgon, J.L. (2011). *Wolbachia* infections are virulent and inhibit the human malaria parasite *Plasmodium falciparum* in *Anopheles gambiae*. PLoS Pathog. *7*, e1002043. https://doi.org/10.1371/journal.ppat.1002043.
15. Lees, R.S., Knols, B., Bellini, R., Benedict, M.Q., Bheecarry, A., Bossin, H.C., Chadee, D.D., Charlwood, J., Dabiré, R.K., Djogbenou, L., et al. (2014). Review: Improving our knowledge of male mosquito biology in relation to genetic control programmes. Acta Trop. *132*, S2–S11. https://doi.org/10.1016/j.actatropica.2013.11.005.
16. Cator, L.J., Wyer, C.A.S., and Harrington, L.C. (2021). Mosquito sexual selection and

reproductive control programs. Trends Parasitol. *37*, 330–339. https://doi.org/10.1016/j.pt.2020.11.009.
17. Charlwood, J.D., and Jones, M.D.R. (1980). Mating in the mosquito, *Anopheles gambiae s.l.* II. Swarming behaviour. Physiol. Entomol. *5*, 315–320. https://doi.org/10.1111/j.1365-3032.1980.tb00241.x.
18. Sawadogo, P.S., Namountougou, M., Toé, K.H., Rouamba, J., Maïga, H., Ouédraogo, K.R., Baldet, T., Gouagna, L.C., Kengne, P., Simard, F., et al. (2014). Swarming behaviour in natural populations of *Anopheles gambiae* and *An. coluzzii*: review of 4 years survey in rural areas of sympatry, Burkina Faso (West Africa). Acta Trop. *130*, 24–34. https://doi.org/10.1016/j.actatropica.2013.10.015.
19. Diabaté, A., Yaro, A.S., Dao, A., Diallo, M., Huestis, D.L., Lehmann, T., Yaro, A.S., Dao, A., Diallo, M., Huestis, D.L., et al. (2011). Spatial distribution and male mating success of *Anopheles gambiae* swarms. BMC Evol. Biol. *11*, 184. https://doi.org/10.1186/1471-2148-11-184.
20. Poda, S.B., Buatois, B., Lapeyre, B., Dormont, L., Diabaté, A., Gnankiné, O., Dabiré, R.K., and Roux, O. (2022). No evidence for long-range male sex pheromones in two malaria mosquitoes. Nat. Ecol. Evol. *6*, 1676–1686. https://doi.org/10.1038/s41559-022-01869-x.
21. Poda, S.B., Nignan, C., Gnankiné, O., Dabiré, R.K., Diabaté, A., and Roux, O. (2019). Sex aggregation and species segregation cues in swarming mosquitoes: role of ground visual markers. Parasites Vectors *12*, 589. https://doi.org/10.1186/s13071-019-3845-5.
22. Manoukis, N.C., Butail, S., Diallo, M., Ribeiro, J.M.C., and Paley, D.A. (2014). Stereoscopic video analysis of *Anopheles gambiae* behavior in the field: challenges and opportunities. Acta Trop. *132*, S80–S85. https://doi.org/10.1016/j.actatropica.2013.06.021.
23. Feugère, L., Gibson, G., Manoukis, N.C., and Roux, O. (2021). Mosquito sound communication: are male swarms loud enough to attract females? J. R. Soc. Interface *18*, 20210121. https://doi.org/10.1098/rsif.2021.0121.
24. Gibson, G. (1985). Swarming behaviour of the mosquito *Culex pipiens quinquefasciatus*: a quantitative analysis. Physiol. Entomol. *10*, 283–296. https://doi.org/10.1111/j.1365-3032.1985.tb00049.x.
25. Ikawa, T., and Okabe, H. (1997). Three-dimensional measurements of swarming mosquitoes: a probabilistic model, measuring system, and example results. In Animal groups in three dimensions, J.K. Parrish and W.M. Hamner, eds. (Cambridge University Press), pp. 90–104. https://doi.org/10.2307/3619124.
26. Manoukis, N.C., Diabaté, A., Abdoulaye, A., Diallo, M., Dao, A., Yaro, A.S., Ribeiro, J.M.C., and Lehmann, T. (2009). Structure and dynamics of male swarms of *Anopheles gambiae*. J. Med. Entomol. *46*, 227–235. https://doi.org/10.1603/033.046.0207.
27. Wu, H.S., Zhao, Q., Zou, D., and Chen, Y.Q. (2011). Automated 3D trajectory measuring of large numbers of moving particles. Opt Express *19*, 7646–7663. https://doi.org/10.1364/OE.19.007646.
28. Khan, Z., Balch, T., and Dellaert, F. (2005). MCMC-based particle filtering for tracking a variable number of interacting targets. IEEE Trans. Pattern Anal. Mach. Intell. *27*, 1805–1819. https://doi.org/10.1109/TPAMI.2005.223.
29. Attanasi, A., Cavagna, A., Castello, L.D., Giardina, I., Jelić, A., Melillo, S., Parisi, L., Pellacini, F., Shen, E., Silvestri, E., and Viale, M. (2015). GReTA - A novel Global and Recursive Tracking Algorithm in Three Dimensions. IEEE Trans. Pattern Anal. Mach. Intell. *37*, 2451–2463. https://doi.org/10.1109/TPAMI.2015.2414427.
30. Butail, S., Manoukis, N., Diallo, M., Ribeiro, J.M., Lehmann, T., Paley, D.A., Ribeiro, M., Lehmann, T., and Paley, D.A. (2012). Reconstructing the flight kinematics of swarming and mating in wild mosquitoes. J. R. Soc. Interface *9*, 2624–2638. https://doi.org/10.1098/rsif.2012.0150.
31. Butail, S., Manoukis, N.C., Diallo, M., Ribeiro, J.M.C., Paley, D.A., Ribeiro, J.M.C., and Paley, D.A. (2013). The dance of male *Anopheles gambiae* in wild mating swarms. J. Med. Entomol. *50*, 552–559. https://doi.org/10.1603/me12251.
32. Cavagna, A., Giardina, I., Gucciardino, M.A., Iacomelli, G., Lombardi, M., Melillo, S., Monacchia, G., Parisi, L., Peirce, M.J., and Spaccapelo, R. (2023). Characterization of lab-based swarms of *Anopheles gambiae* mosquitoes using 3D-video tracking. Sci. Rep. *13*, 8745. https://doi.org/10.1038/s41598-023-34842-0.
33. Shishika, D., Manoukis, N.C., Butail, S., and Paley, D.A. (2014). Male motion coordination in anopheline mating swarms. Sci. Rep. *4*, 6318. https://doi.org/10.1038/srep06318.
34. Qureshi, Y.M., Voloshin, V., Facchinelli, L., McCall, P.J., Chervova, O., Towers, C.E., Covington, J.A., and Towers, D.P. (2023). Finding a husband: using explainable AI to define male mosquito flight differences. Biology *12*, 496. https://doi.org/10.3390/biology12040496.
35. Feugère, L., Gibson, G., Manoukis, N.C., and Roux, O. (2021). Supplementary material from "Mosquito sound communication: are male swarms loud enough to attract females?". R. Soc. Collect. https://doi.org/10.6084/m9.figshare.c.5361985.v1.
36. Feugère, L., Roux, O., and Gibson, G. (2022). Behavioural analysis of swarming mosquitoes reveals high hearing sensitivity in *Anopheles coluzzii*. J. Exp. Biol. *225*, jeb243535. https://doi.org/10.1242/jeb.243535.
37. Maïga, H., Dabiré, R.K., Lehmann, T., Tripet, F., and Diabaté, A. (2012). Variation in energy reserves and role of body size in the mating system of *Anopheles gambiae*. J. Vector Ecol. *37*, 289–297. https://doi.org/10.1111/j.1948-7134.2012.00230.x.
38. Maïga, H., Niang, A., Sawadogo, S.P., Dabiré, R.K., Susan, R., Gilles, J.R.L., Tripet, F., and Diabaté, A. (2014). Role of nutritional reserves and body size in *Anopheles gambiae* males mating success. Acta Trop. *132S*, S102–S107. https://doi.org/10.1016/j.actatropica.2013.08.018.
39. Charlwood, J.D., and Jones, M.D.R. (1979). Mating behaviour in the mosquito, *Anopheles gambiae s.l.* I. Close range and contact behaviour. Physiol. Entomol. *4*, 111–120. https://doi.org/10.1111/j.1365-3032.1979.tb00185.x.
40. Niang, A., Nignan, C., Serge Poda, B., Sawadogo, S.P., Roch Dabiré, K., Gnankiné, O., Tripet, F., Roux, O., and Diabaté, A. (2019). Semi-field and indoor setups to study malaria mosquito swarming behavior. Parasites Vectors *12*, 446. https://doi.org/10.1186/s13071-019-3688-0.
41. Somers, J., Georgiades, M., Su, M.P., Bagi, J., Andrés, M., Alampounti, A., Mills, G., Ntabaliba, W., Moore, S.J., Spaccapelo, R., and Albert, J.T. (2022). Hitting the right note at the right time: Circadian control of audibility in *Anopheles* mosquito mating swarms is mediated by flight tones. Sci. Adv. *8*, eabl4844. https://doi.org/10.1126/sciadv.abl4844.
42. Charlwood, J.D. (2023). Swarming and mate selection in *Anopheles gambiae* mosquitoes (Diptera: Culicidae). J. Med. Entomol. *60*, 857–864. https://doi.org/10.1093/jme/tjad064.
43. Nignan, C., Niang, A., Maïga, H., Sawadogo, S.P., Poda, B.S., Gnankine, O., Dabiré, K.R., Tripet, F., and Diabaté, A. (2020). Comparison of swarming, mating performance and longevity of males *Anopheles coluzzii* between individuals fed with different natural fruit juices in laboratory and semi-field conditions. Malar. J. *19*, 173. https://doi.org/10.1186/s12936-020-03248-y.
44. Diabaté, A., Dao, A., Yaro, A.S., Adamou, A., Gonzalez, R., Manoukis, N.C., Traoré, S.F., Gwadz, R.W., Lehmann, T., Yaro, S.A., et al. (2009). Spatial swarm segregation and reproductive isolation between the molecular forms of *Anopheles gambiae*. Proc. R. Soc. B Biol. Sci. *276*, 4215–4222. https://doi.org/10.1098/rspb.2009.1167.
45. Nignan, C., Poda, B.S., Sawadogo, S.P., Maïga, H., Dabiré, K.R., Gnankine, O., Tripet, F., Roux, O., and Diabaté, A. (2022). Local adaptation and colonization are potential factors affecting sexual competitiveness and mating choice in *Anopheles coluzzii* populations. Sci. Rep. *12*, 636. https://doi.org/10.1038/s41598-021-04704-8.
46. Puckett, J.G., and Ouellette, N.T. (2014). Determining asymptotically large population sizes in insect swarms. J. R. Soc. Interface *11*, 20140710. https://doi.org/10.1098/rsif.2014.0710.
47. Attanasi, A., Cavagna, A., Del Castello, L., Giardina, I., Melillo, S., Parisi, L., Pohl, O., Rossaro, B., Shen, E., Silvestri, E., and Viale, M. (2014). Collective behaviour without collective order in wild swarms of midges. PLoS Comput. Biol. *10*, e1003697. https://doi.org/10.1371/journal.pcbi.1003697.
48. Dabiré, K.R., Sawadogo, P.S., Hien, D.F., Bimbilé-somda, N.S., Soma, D.D., Millogo, A., Baldet, T., Gouagna, L., Simard, F., Lefèvre, T., et al. (2014). Occurrence of natural *Anopheles arabiensis* swarms in an urban area of Bobo-Dioulasso city, Burkina Faso, West Africa. Acta Trop. *132S*, S35–S41. https://doi.org/10.1016/j.actatropica.2013.12.012.
49. Diabaté, A., Baldet, T., Brengues, C., Kengne, P., Dabire, K.R., Simard, F., Chandre, F., Hougard, J.M., Hemingway, J., Ouedraogo, J.B., et al. (2003). Natural swarming behaviour of the molecular M form of *Anopheles gambiae*. Trans. R. Soc. Trop. Med. Hyg. *97*, 713–716. https://doi.org/10.1371/journal.pone.0004549.
50. Gibson, G. (1995). A behavioural test of the sensitivity of a nocturnal mosquito, *Anopheles gambiae*, to dim white, red and infra-red light. Physiol. Entomol. *20*, 224–228.
51. Jolles, J.W., Boogert, N.J., Sridhar, V.H., Couzin, I.D., and Manica, A. (2017). Consistent individual differences drive collective behavior and group functioning of schooling fish. Curr. Biol. *27*, 2862–2868.e7. https://doi.org/10.1016/j.cub.2017.08.004.
52. Santolamazza, F., Mancini, E., Simard, F., Qi, Y., Tu, Z., and della Torre, A. (2008). Insertion polymorphisms of *SINE200* retrotransposons

within speciation islands of *Anopheles gambiae* molecular forms. Malar. J. *7*, 163. https://doi.org/10.1186/1475-2875-7-163.

53. Fry, S.N., Müller, P., Baumann, H.J., Straw, A.D., Bichsel, M., and Robert, D. (2004). Context-dependent stimulus presentation to freely moving animals in 3D. J. Neurosci. Methods *135*, 149–157. https://doi.org/10.1016/j.jneumeth.2003.12.012.
54. Fatou, M., and Müller, P. (2024). 3D video tracking analysis reveals that mosquitoes pass more likely through holes in permethrin-treated than in untreated nets. Sci. Rep. *14*, 13598. https://doi.org/10.1038/s41598-024-63968-y.
55. Feugère, L., Roux, O., and Gibson, G. (2022). Behavioural analysis of swarming mosquitoes reveals high hearing sensitivity in *Anopheles coluzzii*. J. Exp. Biol. *225*, jeb243535. https://doi.org/10.1242/jeb.243535.
56. Bouguet, J.-Y. (2004). Camera calibration toolbox for Matlab.
57. Kalman, R.E. (1960). A new approach to linear filtering and prediction problems. J. Basic Eng. *82*, 35–45. https://doi.org/10.1115/1.3662552.
58. Downes, J.A. (1969). The swarming and mating flight of Diptera. Annu. Rev. Entomol. *14*, 271–298. https://doi.org/10.1146/annurev.en.14.010169.001415.
59. Savitzky, A., and Golay, M.J.E. (1964). Smoothing and differentiation of data by simplified least squares procedures. Anal. Chem. *36*, 1627–1639. https://doi.org/10.1021/ac60214a047.
60. Challis, J.H. (2021). Experimental Methods in Biomechanics (Springer). https://doi.org/10.1007/978-3-030-52256-8.
61. Egelhaaf, M., Boeddeker, N., Kern, R., Kurtz, R., and Lindemann, J.P. (2012). Spatial vision in insects is facilitated by shaping the dynamics of visual input through behavioural action. Front. Neural Circ. *6*, 108. https://doi.org/10.3389/fncir.2012.00108.
62. Srinivasan, M.V., and Zhang, S. (2004). Visual motor computations in insects. Annu. Rev. Neurosci. *27*, 679–696. https://doi.org/10.1146/annurev.neuro.27.070203.144343.
63. Baird, E., Boeddeker, N., Ibbotson, M.R., and Srinivasan, M.V. (2013). A universal strategy for visually guided landing. Proc. Natl. Acad. Sci. USA *110*, 18686–18691. https://doi.org/10.1073/pnas.1314311110.
64. Muijres, F.T., Elzinga, M.J., Melis, J.M., and Dickinson, M.H. (2014). Flies evade looming targets by executing rapid visually directed banked turns. Science *344*, 172–177. https://doi.org/10.1126/science.1248955.
65. Cribellier, A., Straw, A.D., Spitzen, J., Pieters, R.P.M., van Leeuwen, J.L., and Muijres, F.T. (2022). Diurnal and nocturnal mosquitoes escape looming threats using distinct flight strategies. Curr. Biol. *32*, 1232–1246.e5. https://doi.org/10.1016/j.cub.2022.01.036.
66. Cohen, J. (1992). A power primer. Psychol. Bull. *112*, 155–159. https://doi.org/10.1037//0033-2909.112.1.155.

STAR★METHODS

KEY RESOURCES TABLE

REAGENT or RESOURCE	SOURCE	IDENTIFIER
Chemicals, peptides, and recombinant proteins		
Baby fish-food	TetraMin	https://www.tetra.net/en-gb/products/tetramin-baby
Experimental models: Organisms/strains		
Anopheles coluzzii F2 wild type	Institut de Recherche en Sciences de la Sante	N/A
Software and algorithms		
R software (version 4.3.1)	R Foundation	https://www.r-project.org/foundation/
MATLAB (R2017a)	MathWorks	https://www.mathworks.com/
TrackIt3D (version 3.0)	SciTrackS GmbH	N/A
Rmosquito	SPILEn	https://spilen.fr/
R code for statistical analyses	This paper	https://doi.org/10.5061/dryad.8w9ghx3vb
MATLAB code for 3D data analyses	This paper	https://doi.org/10.5061/dryad.8w9ghx3vb
Deposited data		
Databases	This paper	https://doi.org/10.5061/dryad.8w9ghx3vb

EXPERIMENTAL MODEL AND STUDY PARTICIPANT DETAILS

Animals

Experiments were conducted with a newly established (F2) *Anopheles coluzzii* mosquito line. The mosquito line was established from wild females collected in Bama (11° 24′ 14″ N, 4° 24′ 42″ W), a village located 30 km north of Bobo-Dioulasso, Burkina Faso. Indoor-resting gravid females belonging to the *Anopheles* genus were collected using mouth aspirators and transferred to the insectarium. Females were placed individually in oviposition cups containing tap water. After oviposition, females were identified to species by routine PCR-RFLP.[52] Newly hatched larvae from females identified as *An. coluzzii* were pooled. Larvae were reared in tap water and fed *ad libitum* with Tetramin Baby Fish Food (Tetrawerke, Germany). Adult mosquitoes were held in 30 cm × 30 cm × 30 cm mesh-covered cages and provided *ad libitum* with a 5% glucose solution. Insectarium conditions were maintained at a temperature of 27 ± 2°C, a 70 ± 10% relative humidity, and a 12 h:12 h light:dark cycle.

METHOD DETAILS

Video tracking system

We used the Trackit 3D Fly technology platform (SciTrackS GmbH, Bertschikon, Switzerland[53]) to reconstruct the three-dimensional trajectories of the flying mosquitoes. Trackit 3D Fly is a machine-vision-based technology platform conceived to track multiple moving objects in three dimensions with real time monitoring.[23,53–55] The set-up consisted of.

(1) A stereoscopic camera kit including two synchronized digital cameras (Basler acA2040-90um NIR, Germany), operating at 50 frames per second, at an image resolution of 4 megapixels and in the range of near-infrared (NIR) light frequency (CMV4000 CMOS sensor). Each camera was equipped with a Fujinon lens (Fujinon DV3.4 × 3.8SA-SA1, Japan) with which we controlled focus, zoom and aperture, and a NIR band-pass filter (Midwest Optical Systems BP850–25.4, USA) placed between the lens and camera sensor. The filter blocked light outside the NIR wavelength band. The two cameras were connected by a trigger cable to record frames synchronically.
(2) We used four Raytec lamps (Raytec pulsestar illuminators PSTR-I96-HV, United Kingdom) controlled by a controller (PSTR-PSU-4CHNL-HV, UK) to illuminate the tracking area with infrared (IR) light at a wavelength of 850 nm and a power of 880 W. The lights were set to maximal power in constant mode via the controller and the freeware GardasoftMaint (available from www.gardasoft.com). The visual system of mosquitoes is mostly insensitive to NIR light,[50] and thus the use of such lights allows filming the swarming mosquitoes in the dark with minimal disturbance.
(3) The videography tracking system was controlled using a desktop computer (Intel Core i7-8700 CPU @ 3.20 GHz, RAM 16.0 GB, Windows 10), to which the cameras and IR light controller were connected via USB 3.0. On the computer both the tracking software and camera calibration software (MATLAB R2017a, MathWorks Inc) were installed. The stereoscopic camera system was calibrated with the

MATLAB Calibration Toolbox[56] using a checker-pattern board (Pixartprinting, Italy). During experiments, the cameras streamed video to the computer, from which the tracking software reconstructed the three-dimensional flight tracks using a Kalman filtering loop algorithm[57]

Laboratory set-up

The laboratory set-up was located at the Institut de Recherche en Sciences de la Santé (IRSS), Bobo-Dioulasso, Burkina Faso (West Africa). The video tracking system was set up in a room designed to create optimal environmental conditions to trigger *Anopheles* swarming behavior, as described in detail by Niang et al.[40] In summary, the experimental room consisted of a white 5.1 m × 4.7 m × 3.0 m (length × width × height) windowless lab space equipped with a set of hardware for simulating sunset conditions. These included (i) a ceiling light dimmed from maximum light intensity to full darkness in 30 min, (ii) a 0.5 m high black horizon around the complete room perimeter, and (iii) a bright light directed at one of the 5.1 m walls mimicking sunset.

Swarms were produced in a 2.0 m × 0.7 m × 1.8 m (length × depth × height) transparent Plexiglas flight arena, located in the center of the room (Figures 1A and 1B). On one side of the flight arena, we placed a 40 cm × 40 cm black cotton cloth on the floor, which we used as a visual swarm marker. Two synchronized digital cameras (Basler acA2040-90um NIR, 4MP, Germany) were mounted on 0.65 m high tripods and placed close to the sunset wall at 1.35 m from each other and 1.9 m from the flight arena wall. The stereoscopic cameras were placed such that flying mosquitoes could be tracked in three-dimensions across the complete flight arena. Four infrared Raytec lamps (Raytec pulsestar illuminators PSTR-I96-HV, United Kingdom) were fixed on one of the 4.7 m lab walls, above each other (0 m, 0.7 m, 1.1 m and 1.6 m from the floor), at 1.35 m from the flight arena and illuminating the flight arena from the side at a wavelength of 850 nm and a power of 880 W. A desktop computer (Intel Core i7-8700 CPU @ 3.20 GHz, RAM 16.0 GB, Windows 10) to which the cameras and infrared light controller were connected, and on which the tracking software (Trackit 3D, SciTrackS Gmbh, Bertschikon, Switzerland[53]) and camera calibration software (MATLAB R2017a, MathWorks Inc) were installed, was located outside the room, allowing the researcher to assess and control the experiments without having to enter the experimental room.

EXPERIMENTAL DESIGN FOR MOSQUITO FLIGHT RECORDING

Experiments were conducted with a newly established (F2) *An. coluzzii* line from Bama, Burkina Faso (see suppl. Methods for further information). We used four-to-six-day old males of laboratory-reared *An. coluzzii*. For each experiment, we released male mosquitoes into the flight arena 1 h before swarming time, allowing them to acclimatise to the conditions. We chose to release 30 or 50 mosquitoes as this resulted in two swarm sizes of approximately 10 and 20 mosquitoes, respectively. Each swarming experiment was replicated three times. We performed a total of six experimental replicates (*i.e.*, swarms) using a new batch of mosquitoes for each replicate.

At the start of each experiment (*i.e.*, before the mosquitoes were released), both the ceiling and sunset lights were turned on. One hour after the mosquitoes were released, the ceiling lights dimmed slowly from full brightness to off during a period of 30 min. Meanwhile, the sunset light was kept at full power. Approximately 2–3 min after the ceiling lights went off, mosquitoes started to swarm, and the video tracking system was started.

During each experiment, we tracked the swarming mosquitoes at three key phases of the swarming period: (i) at the start of swarming, (ii) at peak swarming, and (iii) at the ending of the swarming activity (Figure 1C). We started the first recording when the first mosquito began flying over the swarm marker, and we continued this recording for 10 min. When the swarm reached its maximal size (~5 min later), we started the second recording, which we continued for 5 min. To capture the decline in swarming activity, we started the third recording 5 min after the end of the second recording. This recording also continued for 5 min.

The tracking system was set to track up to 50 moving objects appearing as bright objects on a dark background, at a temporal resolution of 50 frames per second. The gain, detection threshold, exposure time and minimum object area were set at 5, 10, 10 ms and 20 pixels, respectively. During each data recording period, a video of the flying mosquitoes was recorded using Icecream Screen Recorder software (available from www.icecreamapps.com). These video recordings were used to check and validate the tracking accuracy.

QUANTIFICATION AND STATISTICAL ANALYSIS

Experimental data processing

For each video recording, the tracking software provided a CSV file with the three-dimensional locations (*x,y,z*) of mosquitoes, at a temporal resolution of 20 ms. The coordinate system of the right-handed world reference frame has its origin (0,0,0) on the floor, at the center of the ground marker. The *x*-axis is parallel to the sunset horizon, the *y* axis points toward the sunset, and the *z* axis vertically up. For convenience, we refer to the *z*-coordinates also as *height*. We defined global time *t* as the time relative to the start of swarming (t = 0 s). Furthermore, we defined three time-metrics specific for the swarming phases (t_{start}, t_{peak}, t_{end}, respectively), of which time is zero at the start of the phase-specific video recording (Figure 1C).

The output file contained the data of swarming and non-swarming flights of mosquitoes tracked throughout the flight arena. To select the data of interest (*i.e.*, swarming flights), we plotted for each track the location along the three axes as a function of time, using the Trackit Data Selector program (SciTrackS Gmbh, Bertschikon, Switzerland) running on MATLAB (R2017a). On these graphs, we looked for swarming trajectories as sinusoidal tracks along the three axes (Figures S5A and S5B), as swarming behavior has long been described in the literature as loop-like trajectories.[17,22,24,30,31,58] The swarming tracks were distinct from the non-swarming ones, and were manually selected (Figures S5A

and S5B). To make sure we used data that are characteristic of the start, peak and end of swarming, and to avoid transition phases between these three phases, we selected the swarming flight tracks in the first 450 s, first 150 s and last 150 s of the recordings of the swarm start, peak and ending, respectively (see Figure 1C).

One of the main limitations of video tracking data of mosquito swarms is the interruptions of flight trajectories.[22,30] This results in a significant loss of information of the individual movements in the swarms, and is therefore a limitation in data analyses.[22] For these reasons, we used a specially designed application in Shiny R (*version* 4.3.1) (RMosquito, by SPILEn, France) to automatically reconstruct the interrupted trajectories, wherever possible (see Figures S5C and S5D). The RMosquito program used the principle of clustering to combine segments of interrupted trajectories. According to the three-dimensional spatial and temporal information, a score was established for each track. Then, a hierarchical clustering algorithm grouped the tracks into several clusters according to their score. Finally, the clusters were refined using four user parameters, including (i) minimal track duration, (ii) maximal distance to the nearest track point, (iii) maximal time difference with the nearest track point, and (iv) minimal duration of combined tracks. The reconstructed trajectories were visually checked for combination errors using three-dimensional plots and the video recordings, and the user parameter values were adjusted for correction. After testing several combinations of user parameter values, the following values were used to reconstruct the interrupted swarming trajectories: 0 s, 0.1 m, 0.2 s and 0 s for the minimal track duration, maximal distance to the nearest track point, maximal time difference with the nearest track point and minimal duration of combined tracks, respectively.

For the six experimental replicates (i.e., swarms), we reconstructed in total 13,474 flight tracks (Figure 1E). These tracks were from both flying non-swarming mosquitoes and mosquitoes that exhibited distinct swarming behaviors above the ground marker. Manual selection resulted in the identification of 1,816 swarming tracks, and consecutive automatic stitching of these swarming tracks resulted in a final dataset of 938 swarming flight trajectories (Figures 1F, 1G, S5E, and S5F). The duration of these swarming flight tracks varied from a couple of seconds for the short tracks, to a maximum of 233 s for the longest track. Of these 938 swarming flight trajectories, 60 occurred during the swarm onset phase, 705 during the swarm peak phase, and 173 during swarm ending. This dataset was analyzed to characterize the temporal dynamic of the flight kinematics of individual swarming mosquitoes and, characterize and visualize the three-dimensional shape and structure of the swarms.

Characterising the flight kinematics of individual swarming mosquitoes

The selected and reconstructed tracks were then analyzed in MATLAB R2022b. First, the three-dimensional trajectories were smoothed using a Savitzky-Golay filter,[59] resulting in the smoothed flight trajectory array of positional vectors ($[x(t), y(t), z(t)]$). We then determined the temporal dynamics of velocity ($[u(t), v(t), w(t)]$) and acceleration ($[a_x(t), a_y(t), a_z(t)]$) by taking the first and second temporal derivative of position, respectively. For this, we used a central finite difference scheme of second-order accuracy.[60] From the velocity data, we estimated the flight speed as $U(t) = \sqrt{u(t)^2+v(t)^2+w(t)^2}$, and from the acceleration vectors we estimated the corresponding net acceleration magnitude as $A(t) = \sqrt{a_x(t)^2+a_y(t)^2+a_z(t)^2}$ throughout each flight track. Furthermore, we estimated for each swarming mosquito the distance to closest neighbor at each instant of its swarming flight ($d_{\text{neighbour}}(t)$).

From these kinematics time series, we determined for each swarming mosquito the average and standard deviation of all swarming kinematics parameters. These include per swarming mosquito, the average and standard deviation of location ($(\overline{x},\overline{y},\overline{z}),\sigma(x,y,z)$), flight speed ($\overline{U},\sigma(U)$), acceleration magnitude ($\overline{A},\sigma(A)$), and the average of the distance to closest neighbor ($\overline{d}_{\text{neighbour}}$).

Characterising and visualising the kinematics of the complete swarm

Next to the kinematics of individual swarming mosquitoes, we also quantified the kinematics of the swarm as a whole, to characterise the emergent swarming dynamics that results from the individual flight behaviors. We did this for various subsets of the complete dataset of all swarming mosquitoes: (1) by pooling the flight tracks within the three swarming phases, we reconstructed the emerging swarm kinematics during these three swarming phases separately.

(2) By analysing the subsets for the six separate swarms, we tested how swarming kinematics differed between the studied swarms. (3) Finally, by pooling all 938 swarming flight tracks into a single dataset, we reconstructed the swarm characteristic of a generic swarm of male malaria mosquitoes, in the here-tested lab condition. Note that this generic swarm analysis ignores variations in swarming characteristic between swarms and with time.

For each swarming dataset, we defined the three-dimensional location and spread of the swarm as the average and standard deviation of the positional data of all mosquitoes in the swarm as (x_{swarm} , y_{swarm} , z_{swarm}) and $\sigma(x_{\text{swarm}}, y_{\text{swarm}}$, $z_{\text{swarm}})$, respectively. Furthermore, we quantified the three-dimensional size and shape of the swarms as the volume containing 95% of the detected flight track positions. The remaining 5% of mosquito positions were considered as outliers (i.e., outside the swarm). To do so, we divided the two-dimensional surface of each view (*i.e.*, front, side and top views) into an array of 2 cm × 2 cm cells. Then, we computed the depths that contained 95% of data inside each of these cells (Figures 4A–4C). For this, we estimated the 2.5% and 97.5% quantiles of the third dimension normal to the view of interest (*i.e.*, the *z* dimension when looking at the top view), and we defined the 95% depth as the distance between these two quantiles. Multiplying these depths by the area of cells allowed us to estimate the volume of the swarm that contain 95% of the swarming tracks (Figures 4A–4C).

Within the identified swarm volume, we visualised various swarming metrics using a set of three heatmaps, showing the swarm from the front, side and top (Figures 3, 4, 5, and S9). To do so, we divided the experimental volume into smaller rectangular sub-volumes of 2 cm × 2 cm × *depth* (Figure S11A), and within it we computed metrics such as the number of tracks in each of these sub-volumes

(Figure S11B). Finally, we projected the results of each metric into two-dimensional heatmaps (Figure S11C). We did so for the three orthogonal planes (front, side and top views) to visualise the three-dimensional aspect of mosquito swarming behavior (Figures 3, 4, 5, and S9). The different metrics computed are point and track densities, the average time spent in each sub-volume, mean distance to closest neighbor, mean flight speed, and the mean acceleration magnitude (mean of the vector norm). The point and track density in each sub-volume was estimated as the number of points or tracks per sub-volume, respectively. The average time spent in each sub-volume is defined as $n_{point}/n_{track} \times \Delta t$, where n_{point} is the number of tracked points within a sub-volume, n_{track} is the number of tracks within the volume, and Δt is the time between tracking video frames (0.02 s).

The swarms are found to have quite variable depths depending on the chosen views. Therefore, it is unjust to compare point or track densities in one view to another view (*e.g.*, 60 tracks in a 50 cm deep sub-volume vs. 30 tracks in a 25 cm deep sub-volume). Thus, to better compare metrics between the different two-dimensional views, we normalized point density, track density and average time spent by computing these metrics per cm^3 in each sub-volume that contains 95% of the data (Figures 4D–4L).

Modeling mosquito swarming behavior

In this study, we hypothesised that mosquitoes use visual cues of both the ground marker and sunset horizon to initiate swarming and maintain their position in the swarm. The ground marker can be used by swarming mosquitoes to control their horizontal position (*x*,*y*) and height (*z*) during swarming, and the sunset location allows mosquitoes to orient the main axis of the swarm.

The visual system of insects can accurately decode the optical angular size of objects as an estimate of the apparent size of the objects.[61,62] The angular size of objects scales with the ratio of object size and distance, and so flying insects use optical angular size and its temporal derivative (optical expansion) to control many aspects of flight, including navigation, landing maneuvers, collision avoidance and evasive maneuvers.[63–65]

Here, we hypothesize that swarming mosquitoes use the optical angle of the ground marker as a metric for positioning themselves above the marker, both in height and horizontal location. Moreover, we suggest that mosquitoes also use the retinal position of the sunset to select the angle of view of the marker used to orient the main axis of the swarm (Figure 1D).

To test this hypothesis, we developed a visual-cue-inspired model of mosquito swarming and compared the model output in the form of swarm position, shape and size with the experimental results. The model uses three behavioral rules to define the boundaries of the mosquito swarm (Figure 6A).

(1) The optical angle of the ground marker decreases with increasing flight height, and so for our model we assume that the top and bottom boundaries of the swarm are set by minimal and maximal optical marker angle thresholds perceived by the swarming mosquitoes, respectively.
(2) When a mosquito flies horizontally from a position right above the marker toward the edge of the marker, the optical angle of the marker decreases, thus causing a so-called optic contraction. We suggest that a swarming mosquito uses these optic contraction cues to trigger a turn, causing it to locate above the marker.
(3) The swarming mosquitoes use the optical position of the sunset to orient themselves relative to the sunset, allowing them to discriminate between optical marker angles in the different orientations (parallel and normal to the sunset).

To optimize the swarming model and fit it to the experimental data, we computed the optical marker angles throughout the swarming area and estimated the threshold angles for the model. These are the minimum and maximum optical angle (rule 1), and the reduction in optical angle relative to the maximum at a given height (rule 2). We then assessed the model accuracy by comparing the shapes of the model swarm with the experimental swarm shape.

Based on this comparison, we assessed how well our relatively simple sensory-system inspired model can predict the swarm shape observed in our experiments. Note that this simplified model does not allow us to identify the detailed sensory-motor kinematics that flying mosquitoes use for continue to fly within the swarm. This would require a more complex model, such as an agent-based one.

STATISTICAL ANALYSES OF EXPERIMENTAL DATA

All statistical analyses were performed using R (*version* 4.3.1). We used Linear Mixed-Effects Models (*lmer* function, *lme4* package in R) to test how various motion parameters differ between the three-dimensional axes (*x*,*y*,*z*), the swarming activity phases (start, peak and end of swarming), and the number of swarming mosquitoes at the peak swarming phase. Furthermore, we analyzed the interaction between three-dimensional axes and swarming activity phases (axes × swarming phases) to test whether the *x*, *y* and *z* components of motion parameters varied over the three swarming phases. The motion parameters that we tested were (i) the mean three-dimensional location of the swarming mosquitoes $(\overline{x},\overline{y},\overline{z})$, (ii) the standard deviation of the swarming mosquito location $\sigma(x,y,z)$, (iii) the mean flight speed of the swarming mosquitoes $\overline{U}$, (iv) their mean acceleration magnitude $\overline{A}$, and (v) the mean distance to closest neighbors of the swarming mosquitoes $\overline{d}_{neighbour}$. The experimental swarm numbers (*i.e.*, replicates) were considered as random effects. Additionally, we tested whether these motion parameters differed between experimental swarms (*i.e.*, replicates) using Linear Models (*lm* function, *stats* package in R).

We used Generalized Linear Mixed-Effects Models (GLMMs) with Poisson distributions (*glmer* function, *lme4* package) to test how the number of flying mosquitoes (n_{flying}) and swarming mosquitoes ($n_{swarming}$) differs between swarming phases (start, peak and end phases). Finally, we used a binomial GLMM to test how the proportion of flying mosquitoes that swarm ($R_{swarming} = n_{swarming}/n_{flying} \times 100\%$) differs between the swarming phases (start, peak and end phases). The experimental replicates (i.e., swarms) were considered as random effects.

For model selection, we used the stepwise removal of terms, followed by likelihood ratio tests. Term removals that significantly reduced explanatory power ($p < 0.05$) were retained in the minimal adequate model. Analyses for normality and homogeneity of variances were performed with a Shapiro and Fligner test, respectively (*shapiro.test* and *fligner.test* functions, *stats* package). If necessary, data were transformed using the Box-Cox power transformation method (*powerTransform* function, *car* package).

In addition, we performed analyses on the effect size. The value of partial Eta-squared (η^2) was computed from the full models for each fixed effect (*eta_squared* function, *effectsize* package) and interpreted following the Cohen's rule.[66] Thus, the effect of fixed terms was considered significant when it was both statistically significant ($p < 0.05$) and with a medium or large effect size ($\eta^2 > 0.12$). All statistical results are reported as mean $\pm$ standard error or percentage [95% confidence interval]. For swarm and flight kinematics data, these were estimated from the distribution of mean values of all recorded flight tracks in the test-specific dataset.